FUNDAMENTAL RESEARCH IN SOLID STATE ENERGY CONVERSION PROCESSES

CENTER FOR SPACE RESEARCH

and

Energy Conversion and Semiconductor Laboratory
Department of Electrical Engineering

MASSACHUSETTS INSTITUTE OF TECHNOLOGY
Cambridge 39, Massachusetts

Semiannual Technical Summary Report No. 2
December 1, 1963 to May 31, 1964

on

Contract: NASA Grant NsG 496 (part)
M. I. T. Task: 9827

June 30, 1964

FUNDAMENTAL RESEARCH IN SOLID STATE ENERGY CONVERSION PROCESSES

CENTER FOR SPACE RESEARCH

and

Energy Conversion and Semiconductor Laboratory
Department of Electrical Engineering

MASSACHUSETTS INSTITUTE OF TECHNOLOGY
Cambridge 39, Massachusetts

Semiannual Technical Summary Report No. 2

December 1, 1963 to May 31, 1964

on

Contract: NASA Grant NsG 496 (part)
M.I.T. Task: 9827

June 30, 1964

TABLE OF CONTENTS

PROJECT PERSONNEL

John Blair, Associate Professor of Electrical Engineering

G.S. Almasi, Research Assistant, Electrical Engineering

A.W. Carlson, Research Assistant, Electrical Engineering

J.W. Conley, Research Assistant, Electrical Engineering

P.J. Shaver, Instructor, Electrical Engineering

W. Brennan, Technician

Barbara A. Smith, Secretary

FELLOWSHIP AND THESIS STUDENTS

R.Z. Bachrach

Nguyen Duc Cuong

W.H. Hackett

D.G. Steelman

LIST OF FIGURES

LIST OF TABLES

1.0 INTRODUCTION

During the past reporting period, the activity continued in the areas of photovoltaic, optical, and thermal and electrical properties of materials and material structures. Experiments on aluminum antimonide-gallium antimonide heterojunctions revealed that the photovoltaic response of such structures is governed by a combination of photo-emission and field-emission. Optical measurements of diffused mercury telluride-cadmium telluride graded energy gap structures indicate photovoltaic response at wavelengths well beyond the funadmental absorption of cadmium telluride. Experimental and theoretical work continues to identify the mechanisms contributing to the fundamental optical absorption of cadmium telluride at low temperatures and at room temperature. Additional refinements were introduced in the process of preparing single crystals of zinc antimonide. The apparatus for galvanomagnetic measurements on this material is ready and preliminary data are available. The principal anisotropic thermal expansion coefficients of zinc antimonide have been measured successfully over a broad temperature region with an R.F. dilatometer. Apparatus is being readied for thermal conductivity measurements above room temperature.

In addition to contributions by project personnel, fellowship and thesis students benefited from the association with the staff and facilities of this activity. One S.M. thesis and two S.B. theses were completed by students associated with but not directly supported by the project. A total of two M.S. degrees and two B.S. degrees were granted to students associated with this activity. At the present time, there are five doctoral students and one masters student connected with the project.

The study on the optical properties of cadmium telluride is being made possible through the facilities of the National Magnet Laboratory. The heterojunction work was performed with the cooperation of the staff and facilities of the Lincoln Laboratory.

A.W. Carlson

2.0 PHOTO-FIELD EMISSION IN ALUMINUM ANTIMONIDE-GALLIUM ANTIMONIDE HETEROJUNCTIONS

2.1 Introduction

The photovoltaic effect has been utilized in detectors and energy sources for a number of years.[1,2] The structure of devices utilizing this effect are many and varied, ranging from relatively well understood p-n junctions to not so well understood metal-semiconductor junctions used in commercial photographic exposure meters. By far the most discussed and investigated junctions for photovoltaic energy conversion are the p-n homojunctions of silicon or gallium arsenide.[3,4] With respect to solar cells, the requirements of space exploration have spurred an intense effort towards maximizing the efficiency of present cells and investigating other configurations with ultimately higher efficiencies and improved power to weight ratios of the ultimate space power generating systems.

Recent research on solar cells is concerned with the development of light weight and efficient thin film structures. As opposed to silicon homojunction solar cells, such structures consist of heterogeneous transitions between dissimilar materials. The operation of thin film cadmium sulfide solar cells are governed by processes at or near the heterogeneous transition from cadmium sulfide to copper sulfide or to copper directly. For this reason, the nature of the photovoltaic and electrical properties of an abrupt heterojunction structure was investigated, and the results of this investigation are reported in this chapter.

As opposed to p-n homojunctions,[7,8] p-n heterojunctions are less understood.[5,6] Only recently have attempts been made to treat heterojunctions theoretically since fabrication of such devices is a relatively new development. Anderson[5] and others report on experiments for the fabrication and

evaluation of the electrical properties of heterojunctions. The theoretical models are those due to Perlman[6] and Rediker.[7] Perlman essentially applies a Shockley type diffusion model to the energy distribution across the heterojunction. The voltage-current characteristics are those governed by transport across the smaller barrier. Some anomalies are predicted depending on the magnitude of a forward barrier in the conduction band.

Rediker's theory predicates the operation of the heterojunction on tunneling across the forward barrier rather than thermal transport over it. The basic difference in the I-V characteristics predicted by the two models lies in the temperature dependence of the forward characteristics. The forward characteristics are masked by series resistance effects and non-linear contacts especially at low temperatures therefore experimental interpretation based solely on I-V characteristics measurements have severe limitations.

The interpretation in this paper is based on I-V characteristics, junction capacitance and spectral photovoltaic response measurements. The conclusions are that depending on the height and width of the forward conduction band barrier, either diffusion or tunneling behavior can be observed. It is found, that for thin and high forward barriers, the photovoltaic response is dominated by photo-field emission across the barrier.

2.2 Device Fabrication

The structure that was experimentally investigated is shown in Figure 2.1. AlSb is used as the front face and the junction is illuminated through the AlSb. There is less than one percent lattice mismatch between GaSb (2.64 Å) and AlSb (2.66 Å). Both compounds crystallize in the zinc-blende structure. If properly oriented specimens of AlSb and GaSb are alloyed together the strain and number of dislocations at the interface should be minimal.

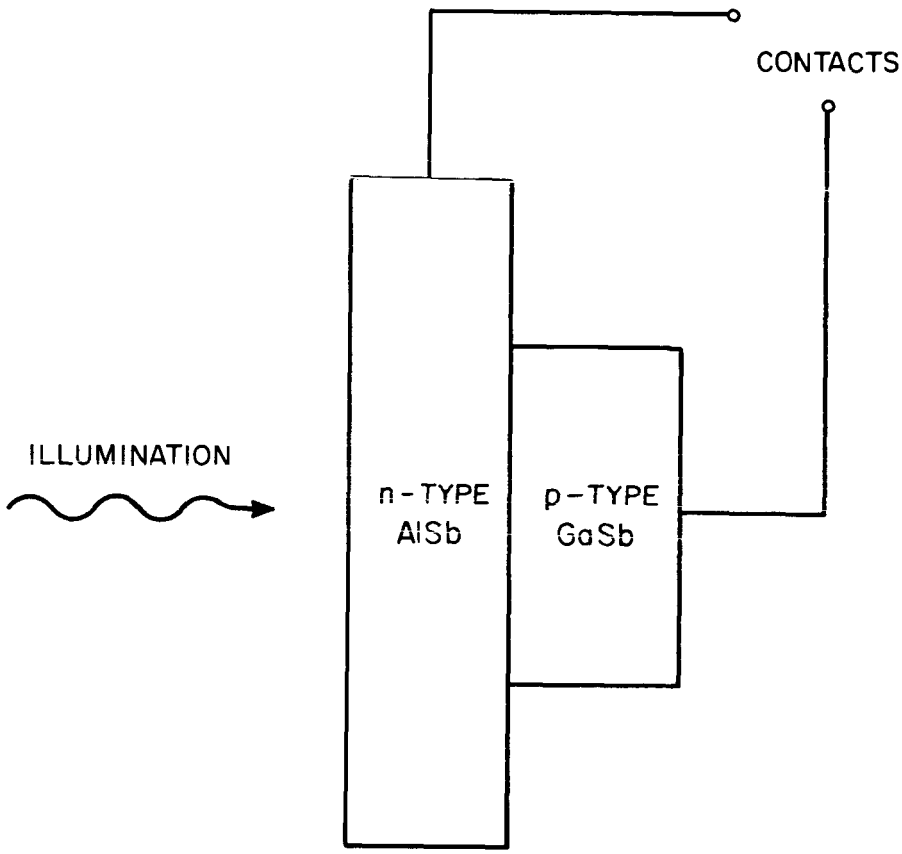

Fig. 2.1 Device Structure Investigated

Three slices of aluminum antimonide were obtained from Bell and Howell Research Center. The slices were Te doped n-type with $n = 1.3 \times 10^{17}$ cm^{-3}, $\mu_e = 191$ cm^2/volt. sec, and $\rho = 0.251$ ohm cm. Although ordered oriented to a (100) plance, the slices obtained were 14° off the (100) plane. Cutting back to the (100) plane meant almost complete loss of usable material as the slices were only a millemeter thick. It was decided to use the crystal slices in their orientation as received.

The slices were polished without the use of water. Lapping paper was used to remove the bulk of the saw damage. Then the slices were polished on a diamond wheel using alcohol and diamond paste to remove all marks. The final polish was obtained using 1/20 micron alumina and alcohol on a synthetic velvet wheel. The final polished slices were .020" thick. For use in fabricating heterojunctions, the polished slices were scored with a diamond scribe and broken into rectangular pieces approximately .150" by .100".

GaSb oriented to a (100) face was obtained from Lincoln Laboratory. The material was undoped p-type with $n = 1.2 \times 10^{17}$ cm^{-3}. The slice was polished on one side and then diced with an ultrasonic cutter into .050" diameter disks.

The melt back technique was used for obtaining an epitaxial junction between the materials. A rectangle of newly etched AlSb was placed on the carbon strip of a hot stage. A newly etched GaSb disk was centered on the face of the piece of AlSb. The hot stage was then closed and flushed with hydrogen gas. To form the junction a current was passed through the carbon strip thus heating the AlSb-GaSb sandwich. Under microscopic observation the sandwich was heated until the GaSb started to melt at the interface. At this point the current was immediately reduced and the GaSb made to re-crystallize. The GaSb does not completely melt and thus remains a single

crystal. The junction forming process takes only seconds and should give a very abrupt junction.

Once the junction is formed there remains only the problem of making contacts to the sample and mounting it on a suitable transistor header. This, however, turned out to be quite a problem. Ohmic contacts were easily made to the GaSb by alloying In-Zn dots using $AlCl_3$ flux and the hot stage. The AlSb surface refused to be even wet by all techniques tried but ultrasonic solder. Attempts to alloy dots of In, In-Te, Sn, Sn-Se, Pb-Sn-Se, Pb-Te failed to wet the surface of AlSb even in the presence of $AlCl_3$ flux. The literature reports that Pb solder can be used for ohmic contacts to AlSb.[8] Finally a process was found which not only wet to AlSb but gave a reasonable ohmic contact. Indium, saturated with tellurium, applied to a heated, freshly cleaved AlSb surface with an ultransonic soldering iron, wet the surface nicely and gave the best contacts obtained. This contact process is very difficult to use on the size scale of the junctions and resulted in a low yield of completed devices.

The samples were then mounted on 4-pin transistor headers with Apiezon W wax. Each device had two contacts to the AlSb and one to the GaSb. Silver ribbon, .002" by .008", plated with indium was used to connect the In-Zn dots and ultrasonic soldered contacts to the header pins.

2.3 Experimental Results

Three complete structures were made using AlSb oriented 14° away from the (100) plane and (100) GaSb. The undersirable 14° mismatch assures the presence of highly strained regions at the interface. The I-V characteristics of the AlSb-GaSb junctions are shown in Figure 2.2. All are reasonably good diodes with saturation current of the order of a few microamps out to -3 volts.

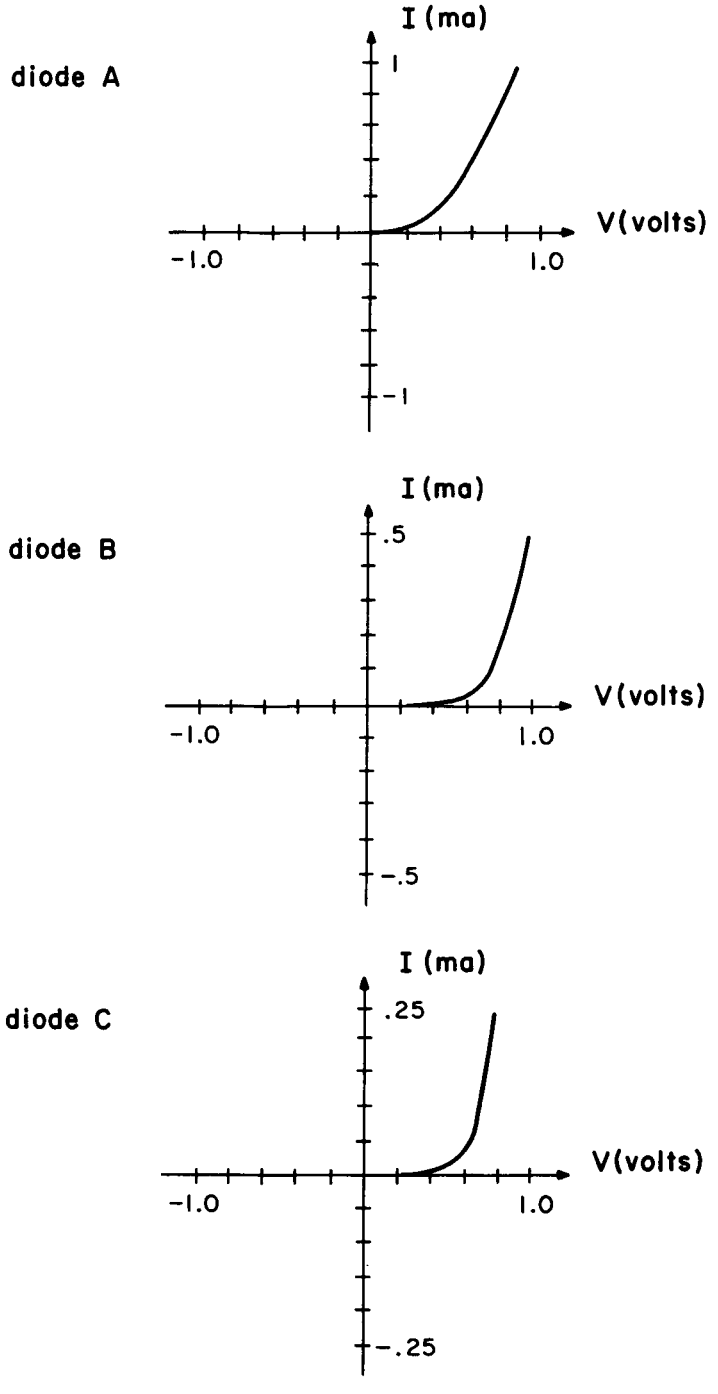

Fig. 2.2 I-V Characteristics of AlSb-GaSb p-n Heterojunctions (300°K)

The diodes start to breakdown sharply in the reverse direction at about -5 volts. Each diode exhibits a different conduction threshold in the forward direction. This is expected as the dislocation and strained area of each junction depends on the depth of the GaSb layer allowed to melt and re-crystallize. These areas govern the exact structure of the barriers at the interface by dislocation doping the interface region. For each diode the junction was biased in the forward direction when the p-type GaSb was positive with respect to the n-type AlSb.

Figure 2.3 shows the I-V relation at 300°K for the diodes with the current plotted on a log scale. Using the equation $\bar{I} = \bar{I}_o \exp q\bar{V}/n\bar{k}T$ to describe the junctions, the following values are obtained for diode A:n = 1.09, diode B:n = 2.23, diode C:n = 2.50. When the measurements were repeated at 77°K the following values of n were obtained: diode A:n = 3.53, diode B:n = 4.00, diode C:n = 3.73. At 77°K, AlSb has a very high resistivity due to either carriers freezing out or mobility becoming very low. Thus series resistance becomes appreciable at low current levels to destroy the simple exponential I-V relation. This causes the log I vs. V plots to be linear only over 2 or 3 orders of magnitude, as opposed to 4 or 5 orders of magnitude at room temperature and makes accurate determination of the slope and n values at T = 77°K virtually impossible. Therefore the liquid nitrogen n values are very approximate.

For each diode, capacitance vs. voltage measurements were made. Figure 2.4 shows the results of these measurements. In Figure 2.4, $1/C^2$ vs. V has been plotted. By simple diode theory the voltage intercept gives an indication of the built-in potential ψ_o for the diode.[6,9] Diode A has a higher saturation current than B or C and its capacitance values were low and

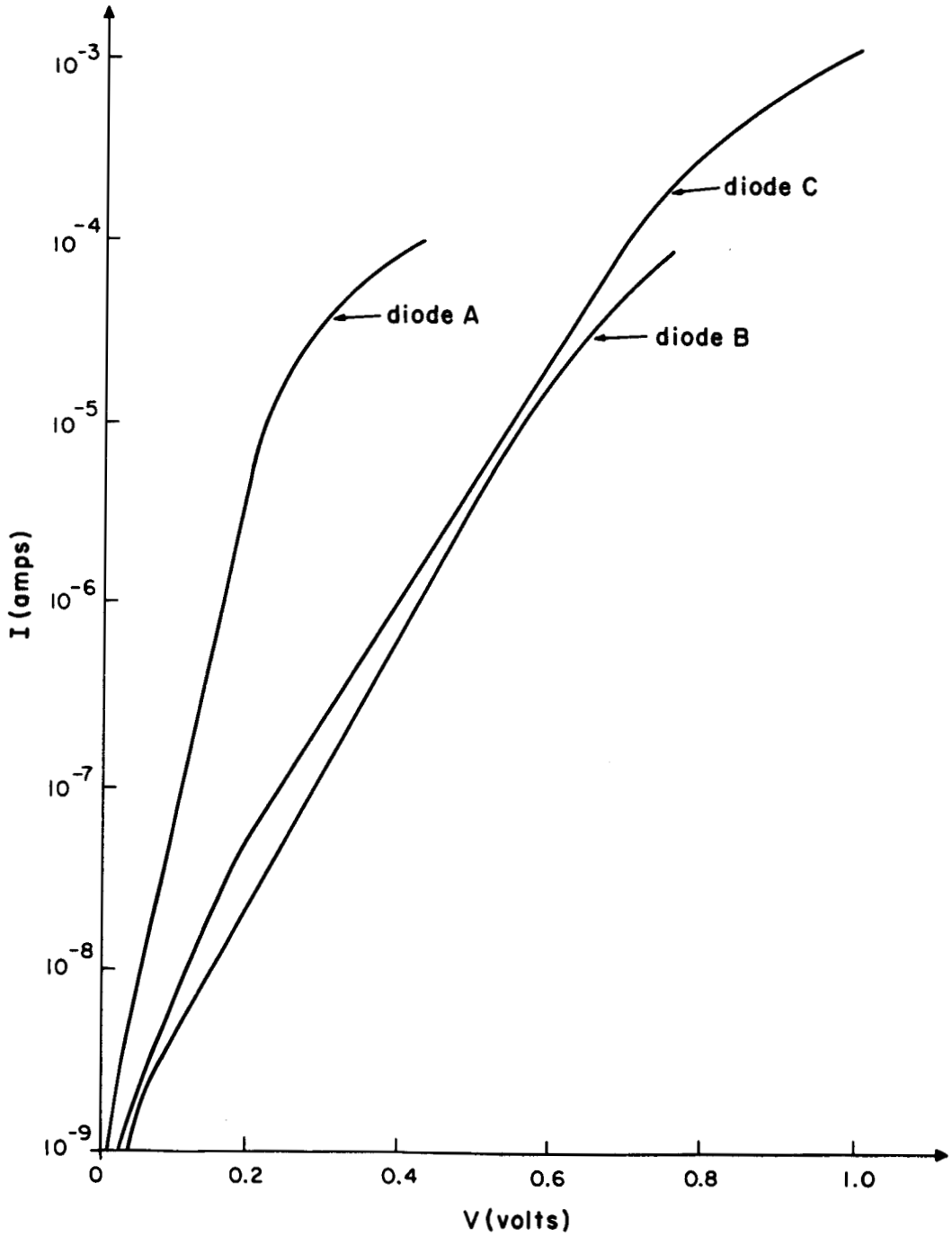

Fig. 2.3 Log I vs. V for AlSb-GaSb Heterojunctions (300°K).

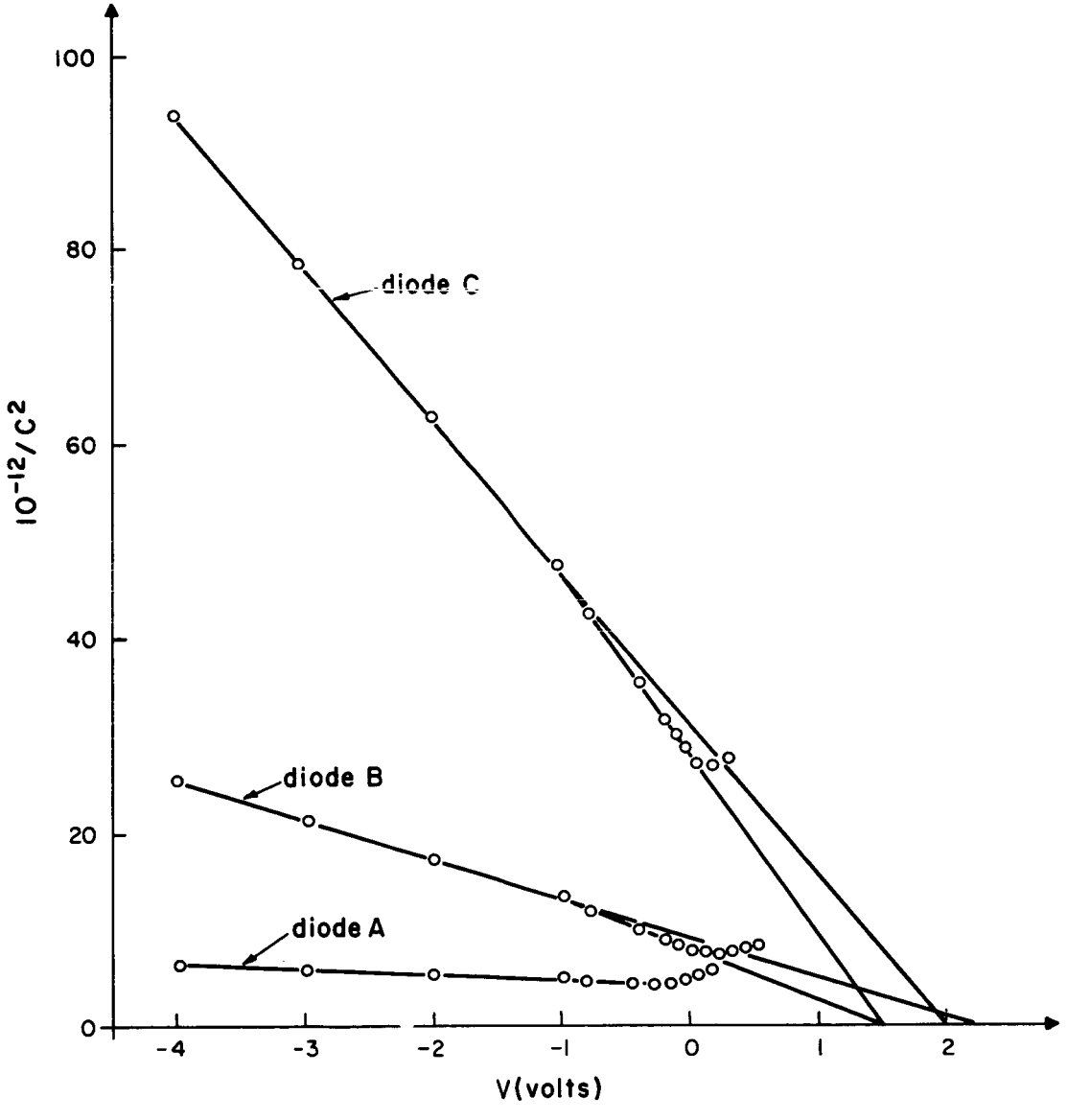

Fig. 2.4 Capacitance vs. Voltage for AlSb-GaSb Heterojunctions (300°K)

of questionable accuracy due to the high conductance. For diodes B and C, the points for each seem to fall on two straight lines. The high reverse bias voltage points indicate a built-in potential of about 2 volts. The points for moderate reverse bias and slight forward bias indicate a built-in potential of about 1.5 volts. In any case, there appears to be a very high built-in potential ψ_o which is indicative of a positive reverse barrier in the conduction band.

When illuminated with a focused microscope lamp, diode A had an open circuit voltage of 100 millivolts. The open circuit voltages of diodes B and C when similarly illuminated were 25 and 20 millevolts respectively. Using a tungsten source and a Perkin-Elmer infrared spectrometer, the spectral open circuit photovoltage was recorded. The output voltage of the hetero-junction was fed directly into the photomultiplier input of the spectrometer's recorder.

Clearly a spectral photovoltaic response should be normalized to equal number of photons incident per unit wavelength. The normal photovoltaic relation is $I_{sc} \approx I_o e^{AV_{oc}}$ where I_{sc} is the short circuit current, A is a constant, and V_{oc} is the open circuit voltage. It was established from transmission measurements that the transmission of photons in the energy range .7 ev. to 1.6 ev. through the AlSb is independent of wavelength. The photons which are transmitted in this energy range are absorbed at the GaSb side of the junction. Because of the high absorption coefficient of GaSb in this energy range, it is assumed that all photons are aborbed well within a diffusion length of the junction. The experimental curves of photovoltage vs. λ must be normalized by dividing the obtained response for a given wavelength by the log of the number of incident photons at that wavelength. If the conditions

listed above are true, the corrected spectral photoresponse curves should be horizontal straight lines between .7 ev. and 1.6 ev. and zero elsewhere providing that all the carriers are collected across the junction. Figure 2.5 shows the corrected spectral photoresponse curves for diodes A, B, and C. The horizontal axis has been changed from wavelength of incident photons to incident photon energy for convenience in later analysis. The photovoltaic response clearly drops off before the transmission threshold of GaSb is reached.

2.4 Conclusions

The capacitance versus voltage data shown in Figure 2.4 indicates an electrostatic built-in potential of about 1.5 volts. This potential value is given by the intercept of a straight line drawn through $1/C^2$ points for voltages centered about V = 0. Table 2.1 lists the predicted and experimentally observed values of n for the three diodes. Using Perlman's thermal model,[6] n should not vary with temperature. The predicted n at 77°K for the diode obeying Redikers tunneling model[7] is $n(77°K) = \frac{300}{77} n\ (300°K)$ i.e. $I = I_o e^{AV}$ where A is temperature independent. From the table it can be seen that diode A obeys Rediker's model fairly well while diodes B and C seem to obey neither model. The high value of built-in potential and the strong deviation from Perlman's model both indicate the presence of a large positive reverse barrier in the conduction band.

From the equation defining K_1 from simple heterojunction theory[5,6] with parameters for the AlSb and GaSb used

$$K_1 = \frac{N_{A2}\epsilon_2}{N_{A2}\epsilon_2 + N_{A1}\epsilon_1} = .5$$

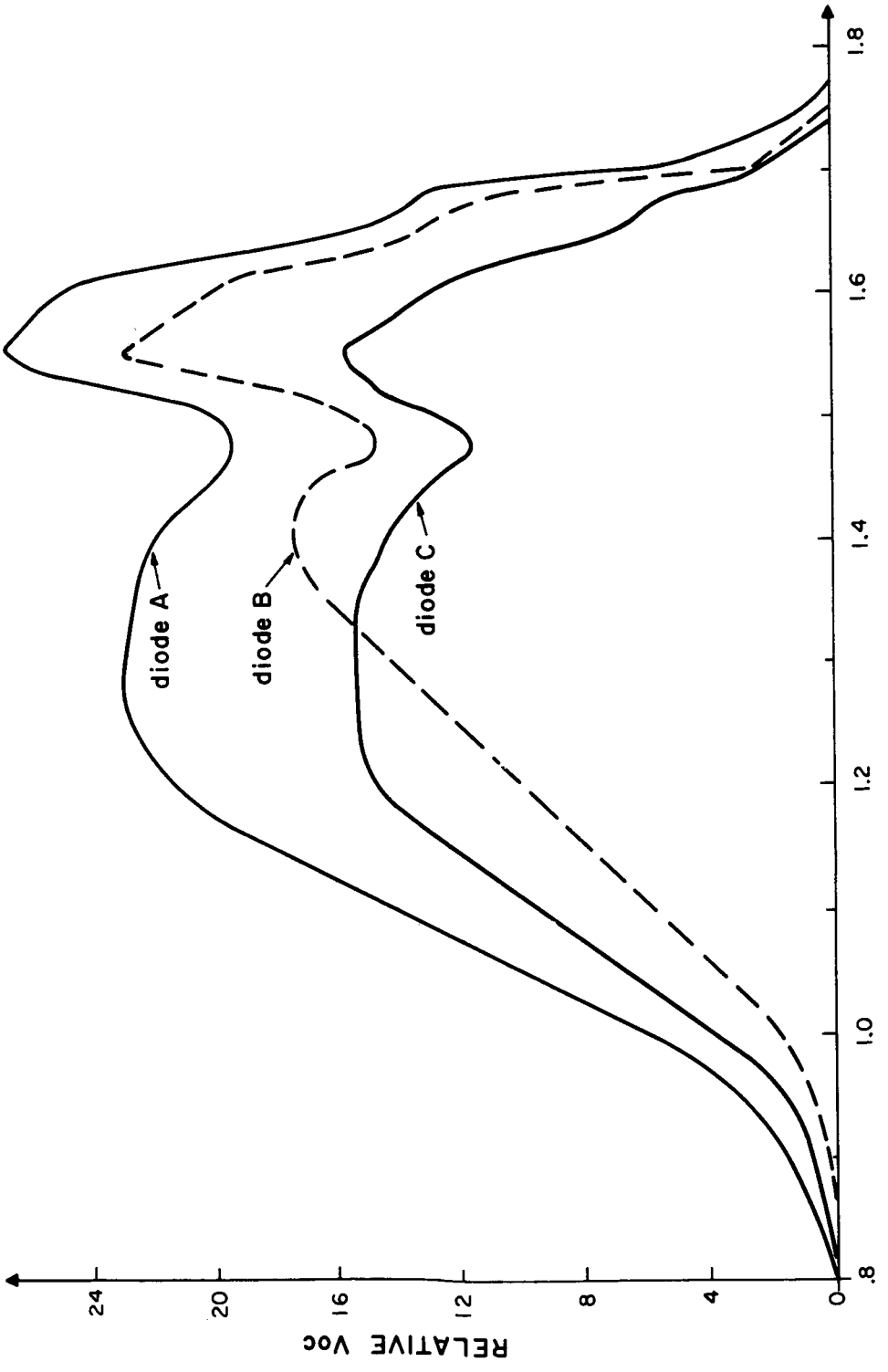

Fig. 2.5 Spectral Photovoltaic Response for GaSb-AlSb Heterojunctions Corrected by Log Number of Incident Photons

	EXPERIMENTAL n		PREDICTED n	
	300°K	77°K	Perlman's model 77°K	Rediker's model 77°K
diode A	1.09	3.53	1.09	4.25
diode B	2.23	4.00	2.23	8.70
diode C	2.50	3.73	2.50	9.75

Note: Predicted n values at 77°K obtained from room temperature experimental values.

Table 2.1 Predicted and experimental variation of n with temperature.

This means that simple theory predicts that half of the electrostatic potential will be supported by each semiconductor. Since simple theory does not account for dislocation doping at the interface this value for K_1 cannot be expected to be very valid. The parameter $q\,\psi_o - \Delta E_c$ (obtained from simple theory) is determined from equilibrium conditions far from the junction and should not be influenced by the details of the interface. At 300°K and using $(N_{c1}/N_{c2}) = (m^*_{e1}/m^*_{e2})^{3/2}$ with the appropriate parameters

$$q\,\psi_o - \Delta E_c = kT \ln \left(\frac{N_{A1}\, N_{A2}}{n_{i2}^2} \right) \left(\frac{N_{c1}}{N_{c2}} \right) \approx .6 \text{ ev}$$

In this calculation n_{i2}^2, the intrinsic carrier concentration squared for GaSb, has been taking as 10^{26} cm^{-3} the value for Ge. This substitution is valid since the two semiconductors have approximately the same energy gap.

Using K_1 and $q\,\psi_o - \Delta E_c$ as calculated and ψ_o equal to 1.5 volts the band structure shown in Figure 2.6 is obtained. Since $K_1 = .5$, AlSb and GaSb each support .75 volts of the built in potential. Taking $q\,\psi_o - \Delta E_c$ as .6 ev., ΔE_c is fixed to be .9 ev. leaving ΔE_v as 0 ev., since $\Delta E_c + \Delta E_v$ must equal $E_{g1} - E_{g2} = .9$ ev. This is the first approximation to the band structure of the junction. Later interpretations of the junctions' optical properties will modify this result.

The spectral photovoltaic response curves shown in Figure 2.5 show several regions of deviation from the expected ideal response. The response for photon energies greater than 1.6 ev. can be attributed to holes collected from photon absorption deep in the AlSb layer. For each diode there occurs a region where the photovoltaic response is reasonably constant. For diode A the region extends from 1.6 ev. down to approximately 1.18 ev. For diode B the region extends from 1.6 ev. down to 1.32 ev. For diode C the region

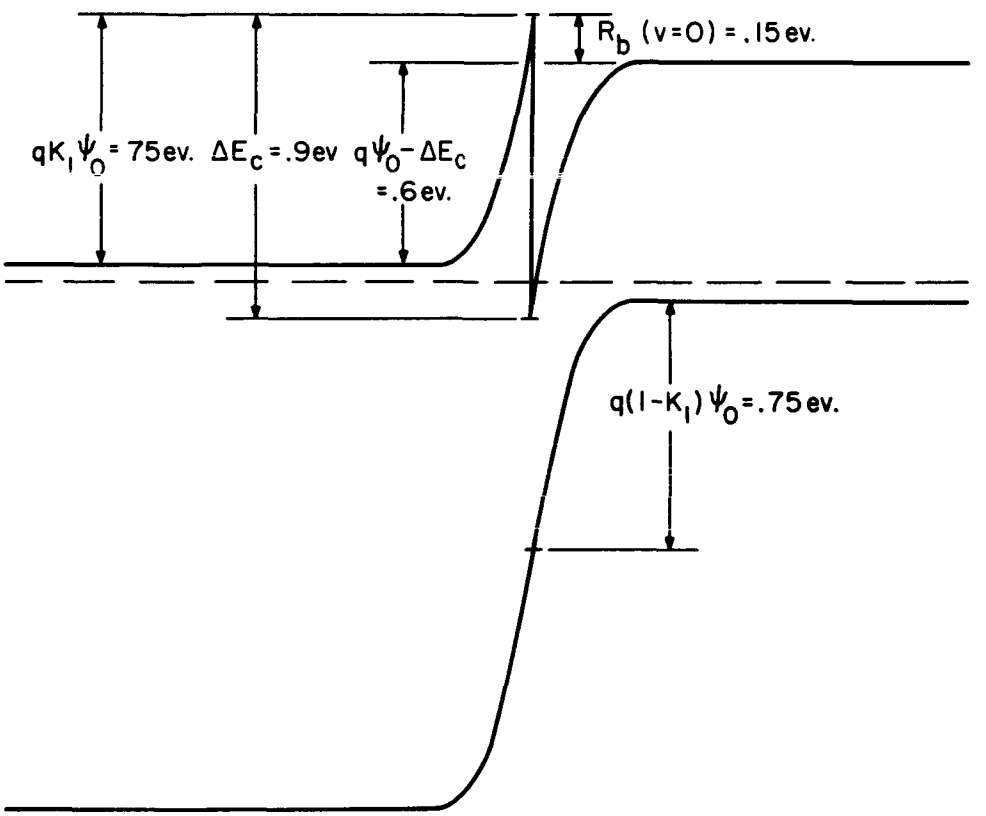

Fig. 2.6 Band Structure of AlSb-GaSb Heterojunction as Determined from Calculated K_1, $q\psi_o - \Delta E_c$, and Experimental ψ_o

extends from 1.6 ev. down to 1.17 ev. For these regions the response is as expected for the ideal case. Immediately following this level region, a region occurs where the photovoltaic response falls off linearly with decreasing photon energy. This occurs for all three diodes. For still lower photon energy the response tails off slowly to zero. A theory is presented below in an effort to explain this behavior.

Field emission of electrons from a cold metal occurs when there is a strong electric field near the surface of the metal.[10] Figure 2.7 shows a form of the potential function near the surface of a metal subject to a strong electric field. Under these conditions electrons near the fermi level are able to tunnel through the barrier and escape from the metal. The tunneling current is observed to obey an expression of the form

$$i = I(\mathcal{E}) \exp[-8\pi(2me)^{1/2} \phi^{3/2}/3h\mathcal{E}]$$

where ϕ is the work function of the metal and $\mathcal{E}$ is the applied electric field.

Photoemission of electrons occurs when a metal is illuminated due to electrons in the metal absorbing a photon and thus gaining enough energy to overcome the work function of the metal and escape from the surface of the metal. Recently photoemission from copper has been shown to contribute to the photovoltaic effect in CdS-Cu photocells.[11] Figure 2.8 illustrates this phenomenon in a metal-semiconductor junction.

With the barrier configurations that occur in heterojunctions a combination of photoemission and field emission may contribute to the photovoltaic effect. With respect to Figure 2.9 consider electron-hole pairs generated at point A by photons of energy $h\nu$. If the photon is absorbed by an electron near the top of the valence band, the generated conduction electron will have

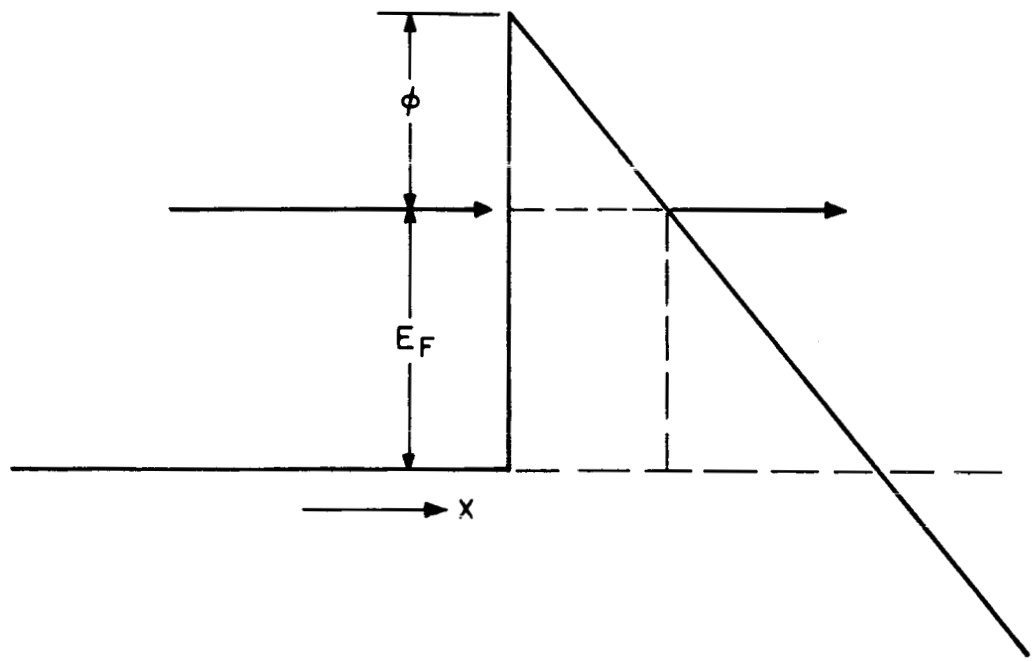

Fig. 2.7 Potential Function Near the Surface of a Metal Subject To a Strong Electric Field

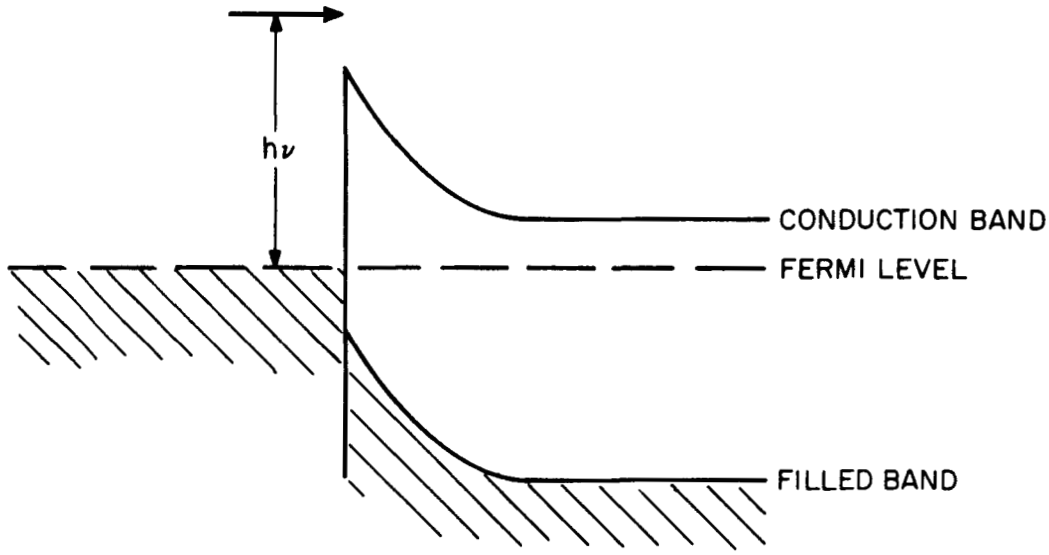

Fig. 2.8 Configuration of Energy Bands For a Metal-Semiconductor Junction Showing Process of Photoemission Contributing To Photovoltaic Effect

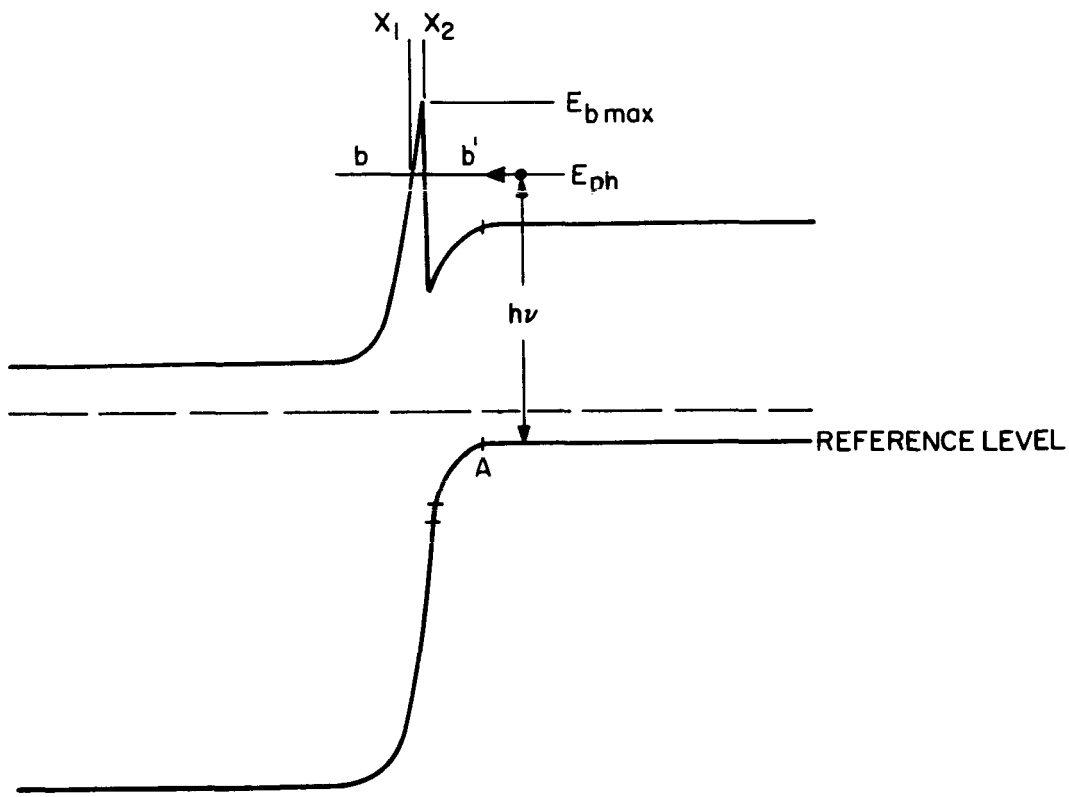

Fig. 2.9 Optically Generated Conduction Electron Incident On Barrier Of Heterojunction

an energy hν above the top of the valence band. The junction field will draw the electron towards the barrier region. If the energy of the electron is greater than the maximum energy of the barrier, the electron can easily go over the barrier and cross the transition region thus contributing to the photovoltaic effect. However, if the energy of the electron is less than the maximum energy of the barrier, the electron will either be stopped by the barrier or tunnel through the barrier and cross the transition region. An electron stopped by the barrier would not contribute to the photovoltaic effect whereas an electron that tunneled through the barrier would.

The probability of an electron tunneling through the barrier may be calculated using the WKB approximation.[10]

$$t = \exp\left\{-2 \int_{x_1}^{x_2} [2m_e^*(E_b(x) - E_{ph})]^{1/2} \frac{dx}{\hbar}\right\} \qquad (1)$$

In writing equation (1) it has been assumed that the electron tunnels through the barrier along a path bb' in Figure 2.9. E_{ph} is the photon energy with which the electron was excited from the valence band. $E_b(x)$ is the energy of the barrier as a function of distance using the valence band on the smaller gap side as a reference for E = 0. Thus $[E_b(x) - E_{ph}]$ is the height of the barrier as a function of distance that the excited electron sees. Assuming a constant field F_o in the barrier region, $E_b(x)$ will be given by $F_o x$ where $F_o x_1 = E_{ph}$ and $F_o x_2 = E_{b\ max}$. Then

$$t = \exp\left\{-\frac{2\sqrt{2m_e^*}}{\hbar} \int_{x_1}^{x_2} \sqrt{F_o x - E_{ph}}\ dx\right\} = \exp\left\{-\frac{4\sqrt{2m_e^*}}{3\hbar F_o} [E_{b\ max} - E_{ph}]^{3/2}\right\}$$

$$\approx \exp\left\{-\frac{4\sqrt{2m_e^*}}{3\hbar F_o} E_{b\ max}^{3/2}\right\} \exp\left\{\frac{2\sqrt{2m_e^*}}{\hbar F_o} (E_{b\ max})^{1/2} E_{ph}\right\} \qquad (2)$$

for small $[E_{b\ max} - E_{ph}]$. Writing E_{ph} as $E_{b\ max} - \Delta E$ equation (2) becomes

$$t \approx \text{const}\ e^{-B\Delta E} \tag{3}$$

where B equals a constant and ΔE is the energy difference between the top of the barrier and the excited electron.

Going back to the spectral photovoltaic response curves of Figure 2.5, the linear decrease of photovoltage with photon energy which occurs for each diode may be explained with the above theory. The absorption coefficient for GaSb is about 10^5 for photons in this energy range so that the bulk of the electron-hole pair generation will occur within the first 0.1 microns of GaSb. The high field in this region forces the generated electrons towards the interface where they either go over, tunnel through, or are stopped by the barrier. Assuming the photons are absorbed by electrons near the top of the valence band and the electrons do not suffer enough collisions to change their initial energy distribution before reaching the interface, a monochromatic photon source will generate electrons that are in a narrow band of energy $h\nu$ above the valence band when they reach the interface. For incident photons which generate electrons ΔE below $E_{b\ max}$ the photovoltaic effect will be, using equation (3)

$$I_{sc} = C\ e^{-B\Delta E} = I_o\ e^{AV_{oc}}$$

Thus V_{oc} will decrease linearly as ΔE increases or as $h\nu$ of the incident photons decreases.

This behavior is exhibited by each of the three diodes. The photon energy initiating this decrease in V_{oc}, due to the electrons having to tunnel through the barrier, gives the energy difference between the barrier peak and the valence band of GaSb.

Once the energy of the incident photons is low enough to force electrons generated in the GaSb to tunnel through the barrier for collection, further decrease in photon energies forces the electrons to tunnel through higher and higher barriers. Thus the number of generated electrons that are collected becomes smaller and finally vanishes. For very small I_{sc} the assumed photovoltaic relation $I_{sc} = I_o e^{AV_{oc}}$ no longer holds. Instead the full diode relation $I = I_o(e^{AV_{oc}} - 1)$ must be used and $I_{sc} = I_o(e^{AV_{oc}} - 1) \approx I_o AV_{oc}$. The linear relation of I_{sc} and V_{oc} for small V_{oc} accounts for the "tails" on the photovoltaic response curves of Figure 2.5 following the linear decrease due to the reverse barrier.

The onset of the tunneling behavior gives a good indication of the reverse barriers actually present in the diodes. This information can be used to predict the band structure of the junction with more accuracy than before when K_1 was used. From Figure 2.5, $h\nu$ at the onset of tunneling is 1.17 ev., 1.32 ev., and 1.18 ev. for diodes A, B, and C respectively. Taking 1.2 ev. as typical for the diodes, the reverse barrier extends .5 ev. above the conduction band of GaSb. Using $\psi_o = 1.5$ ev. and $q\psi_o - \Delta E_c = .6$ ev. from the earlier calculation, the band structure shown in Figure 2.10 is obtained.

With regards to solar cell performance, a heterojunction with a high reverse barrier has poor collection properties for electrons or holes generated by photons of energy just above the energy gap of the smaller gap material. On the other hand a high reverse barrier device should give a higher open circuit voltage for a given short circuit current than the same device with a smaller barrier. Thus the advantages and disadvantages of reverse barriers in heterojunction photo devices must be resolved for each

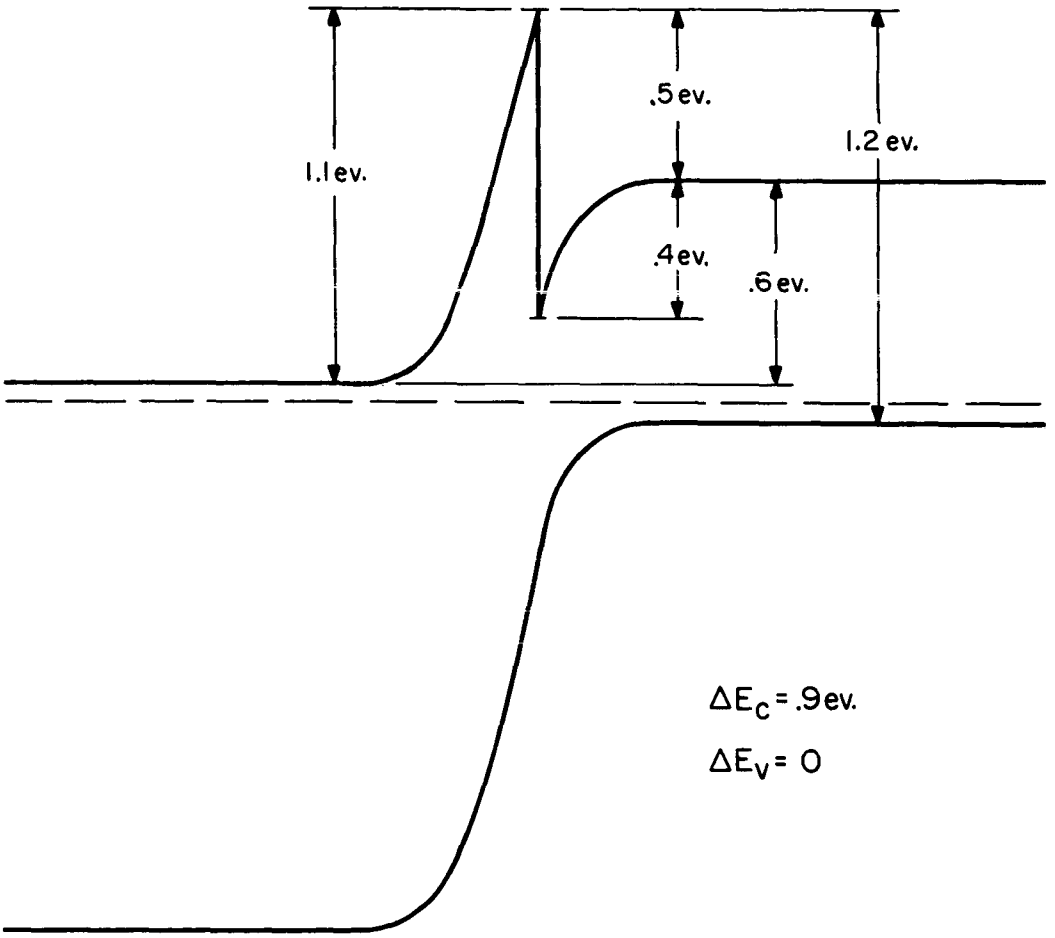

Fig. 2.10 Band Structure of AlSb-GaSb Heterojunction as Determined From Calculated $q\psi_o - \Delta E_c$, Experimental ψ_o, and Experimental Reverse Barrier

application by comparison of junction spectral response and intended input spectrum.

To date, the work that has been done on heterojunctions is only a small step towards the understanding of heterojunctions and heterojunction devices. All the existing theories on such junctions are relatively unproven.

The present work has shown the importance of the reverse barrier in heterojunctions in photovoltaic performance. Further, the importance of photo response measurements has been illustrated for determining the barrier structure in heterojunctions.

Most of the experimental work described was done using the facilities of Lincoln Laboratory. The author is grateful to Dr. R.H. Rediker and the personnel of Group 85 at Lincoln Laboratory for their cooperation with the experimental work and for making available a preprint of their forthcoming paper.

2.5 Bibliography

1. P. Rappaport, "The Photovoltaic Effect and its Utilization", RCA Review, V. 21, p. 373 (1959).

2. D.C. Reynolds, G. Leiess, L.L. Antes, and R.E. Marburger, "Photovoltaic Effect in CdS", Physical Review, Vol. 96, p. 533 (1954).

3. T.S. Moss, "The Potentialities of Silicon and Gallium Arsenide Solar Batteries", Solid-State Electronics, Vol. 2, p. 222 (1961).

4. M. Prince, "Silicon Solar Energy Converters", J. Appl. Physics, Vol. 26, p. 534 (1955).

5. R.L. Anderson, Germanium-Gallium Arsenide Contacts, Ph.D. Thesis, Syracuse University, 1960.

6. S. Perlman, P-N Heterojunctions, Ph.D. Thesis, Carnegie Institute of Technology, 1963.

7. R.H. Rediker, S. Stopek and J.H.R. Ward, "Interface-Alloy Epitaxial Heterojunctions", to be published in Solid State Electronics.

8. A. Herczog, R.R. Haberecht, and A.E. Middleton, "Preparation and Properties of Aluminum Antimonide", Journ. Electrochem. Soc., 105, 533 (1958).

9. Jonscher, Principles of Semiconductor Device Operation, Wiley, 1960.

10. R.A. Smith, Wave Mechanics of Crystalline Solids, Chapman and Hall, 1961.

11. R. Williams and R. Bube, "Photoemission in the Photovoltaic Effect in Cadmium Sulphide Crystals", Journal of Applied Physics, 31 968, (1960).

3.0 GRADED ENERGY GAP HETEROSTRUCTURES

3.1 Introduction

A series of preliminary optical measurements on a graded energy gap device has just been completed, and the results are in the process of being analyzed. However, it may be interesting to give a preview of these results.

3.2 Experimental Results

The device was made by diffusing HgTe into a CdTe wafer. The metallurgical characteristics of such a structure were described in an earlier report.[1] Indium soldered contacts were placed as shown in Figure 3.1 to minimize contributions to the photovoltage due to CdTe alone. The wavelength region between 0.5 and 10 microns was investigated for temperatures between 1.7°K and 300°K and for magnetic fields up to 20 kilogauss.

Figure 3.2 shows the spectral dependence of the magnetic-field-dependent photovoltage (the P.E.M. voltage) at 16.4 kilogauss and 120°K. (The photovoltage has been normalized by dividing by the number of incident photons in each wavelength internal.) Figure 3.3 shows how the un-normalized P.E.M. voltage depends on magnetic field for several different wavelengths.

3.3 Discussion

The interpretation of results as these is not a simple matter. However, if it is assumed that the simplifying assumptions in the author's earlier analysis[2] of such a device can be made, then it is possible to make several interesting conjectures.

The analysis referred to above showed that the normalized spectral response should be directly proportional to magnetic field and energy-gap gradient and to a position-dependent "effective mobility" and lifetime; it should be inversely proportional to the "dark" carrier concentration.

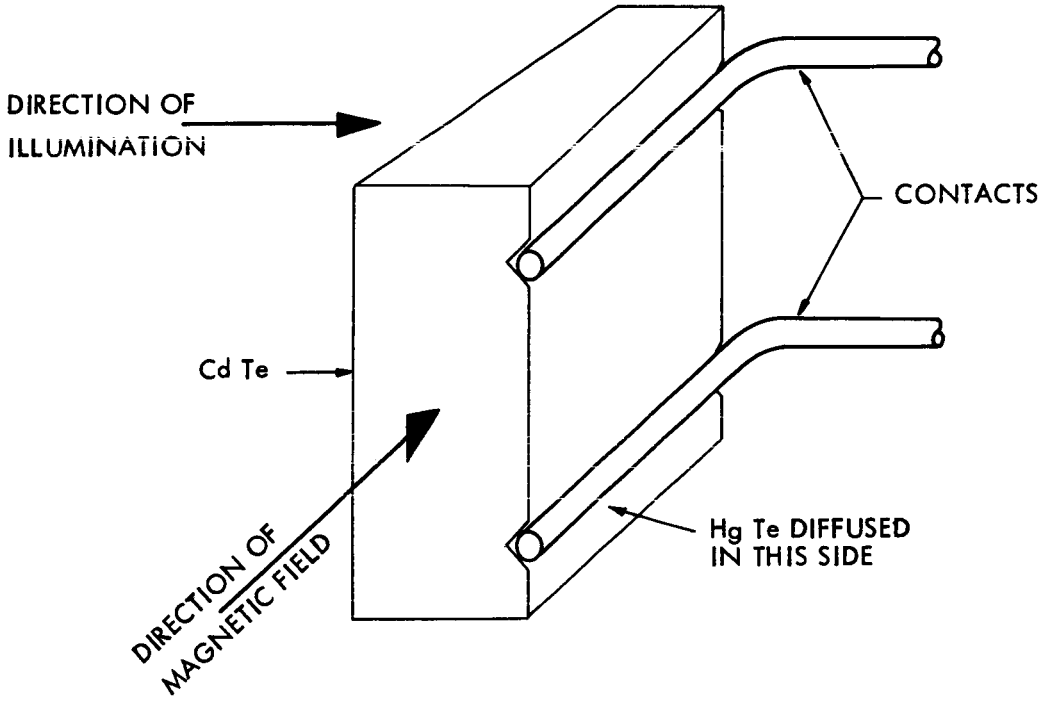

Fig. 3.1 Sample Geometry

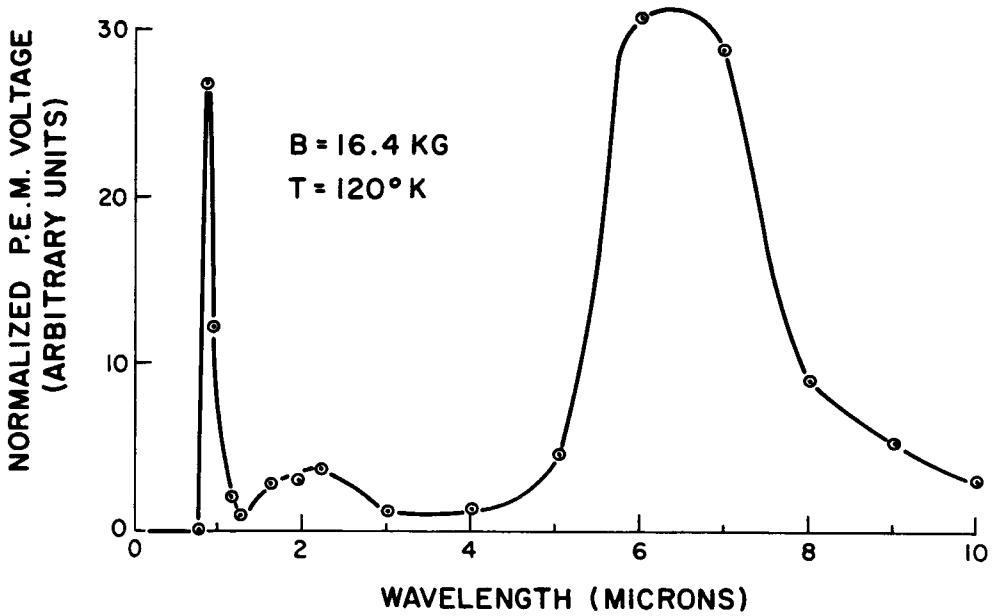

Fig. 3.2 Normalized P.E.M. Voltage Of Sample B2098 02 No. 2

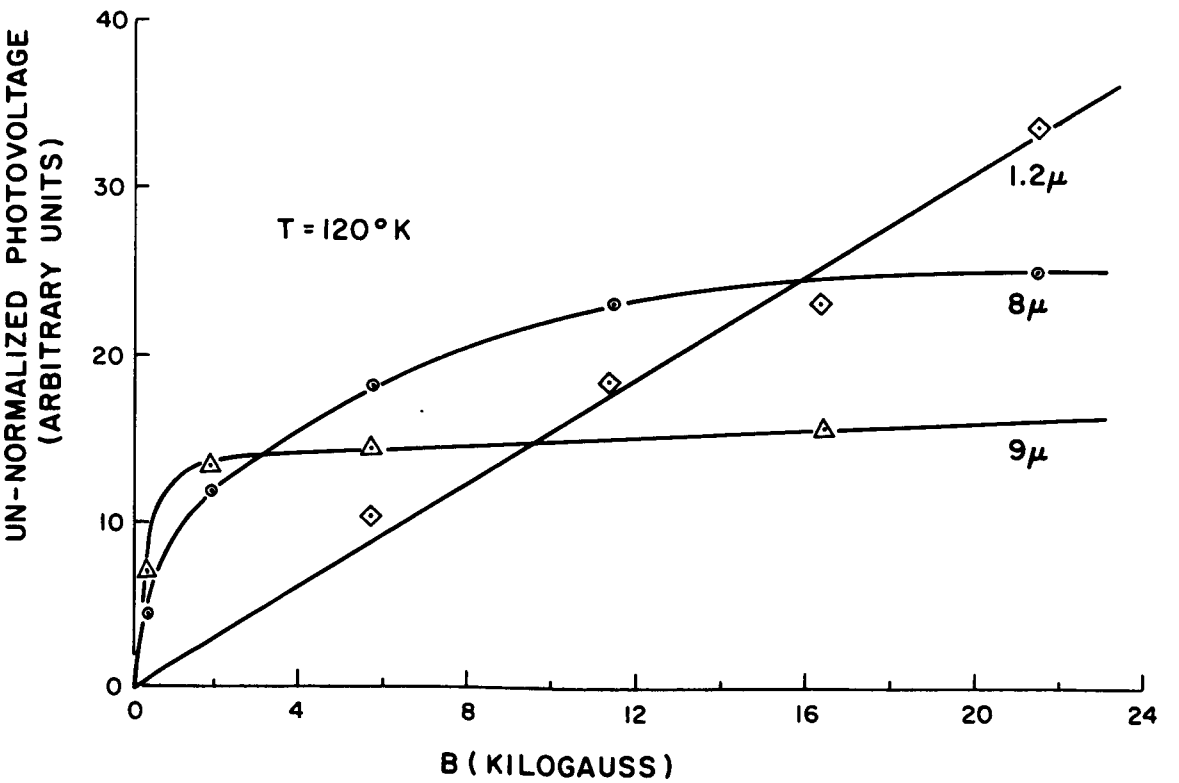

Fig. 3.3 Magnetic Field Dependence Of P.E.M. Voltage Sample B2098 02 No. 2

Although the energy-gap gradient can be inferred from the metallurgical measurements, this still leaves variations in mobility, lifetime, and carrier concentration as possible causes for the shape of the spectral response. However, it may be possible to eliminate one of these unknowns.

An examination of Figure 3.3 shows the interesting fact that the value of magnetic field for which saturation occurs varies with wavelength and thus with the energy-gap region being considered. The analysis in the previous reference was carried out under the assumption that $B\mu<<1$ everywhere (B = magnetic field strength, μ = mobility), but further analysis would show some kind of saturation or perhaps a maximum for $B\mu=1$. Thus in a very crude way it is possible to infer the behavior of the mobility from a plot such as Figure 3.3. This would imply that the mobility in the portion of the device having an absorption edge of 9 microns is at least 50,000 cm^2/v-sec, since the effect is well saturated at B = 2 kilogauss, whereas the corresponding value for 1.2 microns is less than 4,000 cm^2/v-sec, since no saturation is evident up to B = 25 kilogauss.

These results are not inconsistent with the results of Lawson and Nielsen[3] on bulk samples of HgCdTe, who find a value at 77°K of 209 cm^2/v-sec for a sample with absorption edge at 2 microns, and 26,400 cm^2/v-sec for a sample with an absorption edge at 9.4 microns. The results of Figure 3.3 would further say that the decrease in spectral sensitivity between 8 microns and 9 microns (Figure 2) is <u>not</u> due to a decrease in mobility.

It must be re-emphasized that the above conclusions are tentative and are based on an incomplete analysis of the data. This analysis is under way and will be completed shortly. After that, it is planned to fabricate devices under different conditions and to set up a more systematic optical measurement procedure.

3.4 Bibliography

1. Semi-annual Technical Summary Report No. 2, "Research on Materials, Processes, and Devices Related to Energy Conversion", Contract No. Nonr-1841(78), March 30, 1962, pp. 53-58.

2. G.S. Almasi, "HgTe-CdTe Graded-Gap Device", M.S. Thesis, M.I.T., 1962.

3. W.D. Lawson et al, "Preparation and Properties of HgTe and Mixed Crystals of HgTe-CdTe", J. Phys. Chem. Solids 9, 325 (1959).

J.W. Conley

4.0 THE OPTICAL ABSORPTION EDGE IN CADMIUM TELLURIDE

4.1 Introduction

Single crystal CdTe obtained from the process described earlier[1] has been examined in optical transmission and the results subjected to theoretical analysis. The mechanism affecting absorption at the steeply rising edge at low temperatures has been identified as arising from the creation of an exciton with the simultaneous destruction of the photon and a LO phonon.[2,3] A similar conclusion has been reached by Marple and Segall in a recent and independent investigation.[4,5,6] There are, however, contrasts both in the experimental and in the theoretical results of the two studies, discussed below, which lead one to question the validity of the "state of the art" understanding of this effect.

In the course of the optical experimentation at low temperatures and in high magnetic fields no evidence for indirect transitions hence the existence of a "many valley" conduction band as proposed by Davis and Shilliday[7] and by Konak[8] was obtained. It is becoming gradually more clear what the mechanisms responsible for the absorption at temperatures below liquid nitrogen are; however, the situation above this range is not yet interpreted.

Several interesting theoretical results have been obtained. The second order time dependent absorption theory[9] upon which calculations for the optical absorption involving phonons is generally calculated has been shown to be in conceptual error. Results previously based on this theory may be quantitatively correct to a somewhat lesser degree than previously supposed, however, this is not generally so. A theory for a process which is similar in many respects to the LO phonon assisted absorption by excitons previously

derived by the others has been developed in which the TO phonon modes are shown to contribute significantly to the absorption at low temperatures.

4.2 The Experimental Evidence for LO Phonon Assisted Absorption by Excitons

With the optical equipment which was available earlier in this investigation the high magnetic field search for oscillatory behavior[10] in absorption which could have been due to indirect transitions produced no evidence to substantiate this mechanism. The zero field data and a data sequence at several low temperatures on a single sample is, however, interpreted. On a carefully polished sample from an ingot of good optical quality the data shown in Figure 4.1 was obtained. Also shown are the exciton positions obtained by fluorescent emission.[11] The sample thickness was 129 microns. Material from this ingot showed no band like absorption to shallow levels which had been observed in earlier measurements. No free carrier absorption or other anomalies in the infrared spectrum from 2 to 15 microns which had also been observed on the earlier ingots was present. Because of the absence of free carriers transport evaluation of the material parameters could not be made. Data at the lower temperatures normalized with respect to the temperature dependent exciton energy, E_o, is shown in Figure 4.2. A temperature independent component is displayed. When this is subtracted from the data at higher temperatures and which is subsequently normalized with respect to the Bose occupation factor of the LO phonon modes, $\bar{n}$, the results given in Figure 4.3 are obtained. This presentation which is similar in form to that obtained in the studies of ZnO[3] and CdS[4] is interpreted as indicating the interaction of the LO phonons and excitons. However, a comparison with equivalent data of Marple[6] (Figure 4.4) shows that their absorption coefficient, $\alpha(h\nu)$, is a factor of 20 higher in magnitude. The

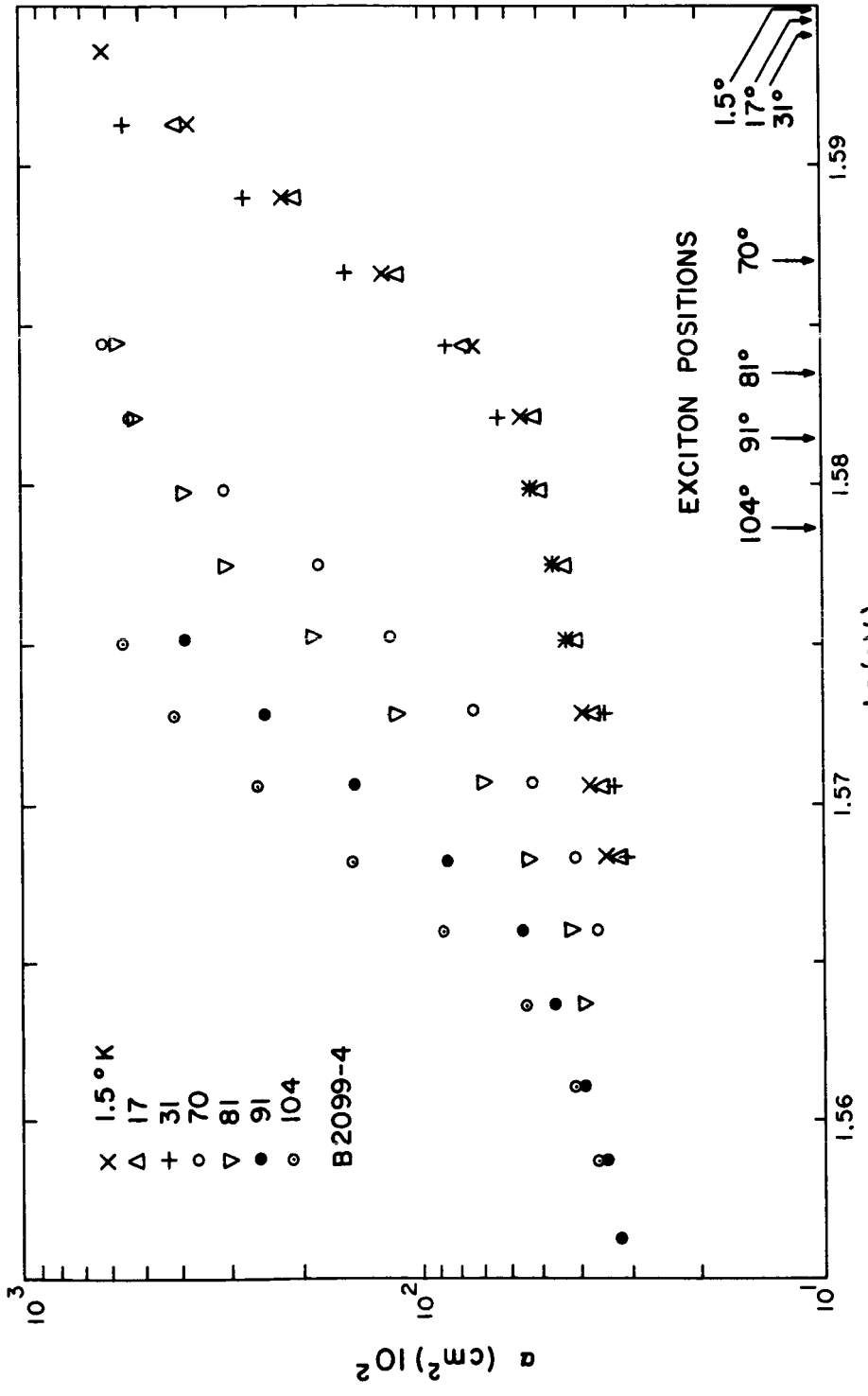

Fig. 4.1 Low Temperature Data For Sample B2099-4

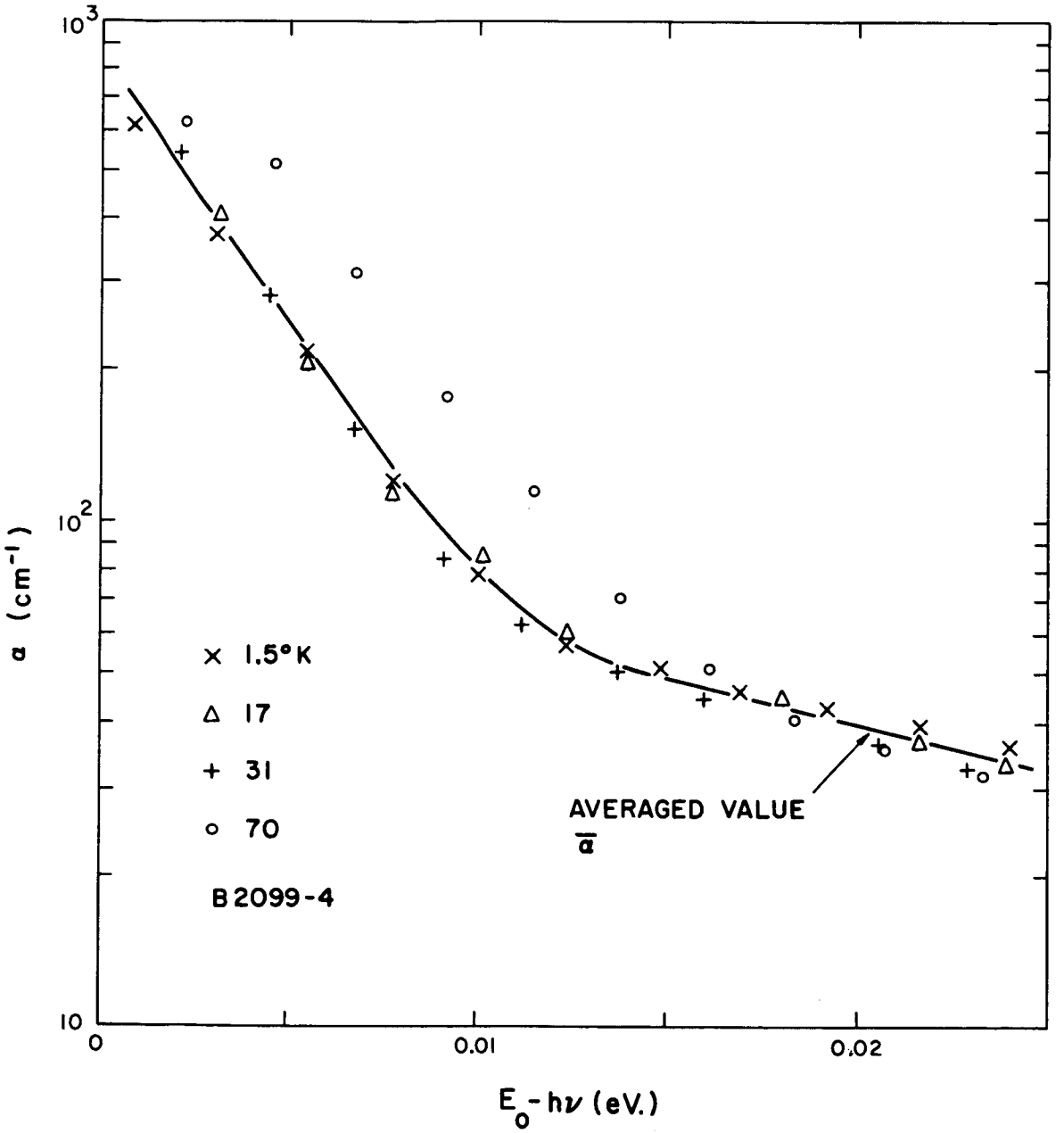

Fig. 4.2 Normalized Absorption at Lower Temperatures

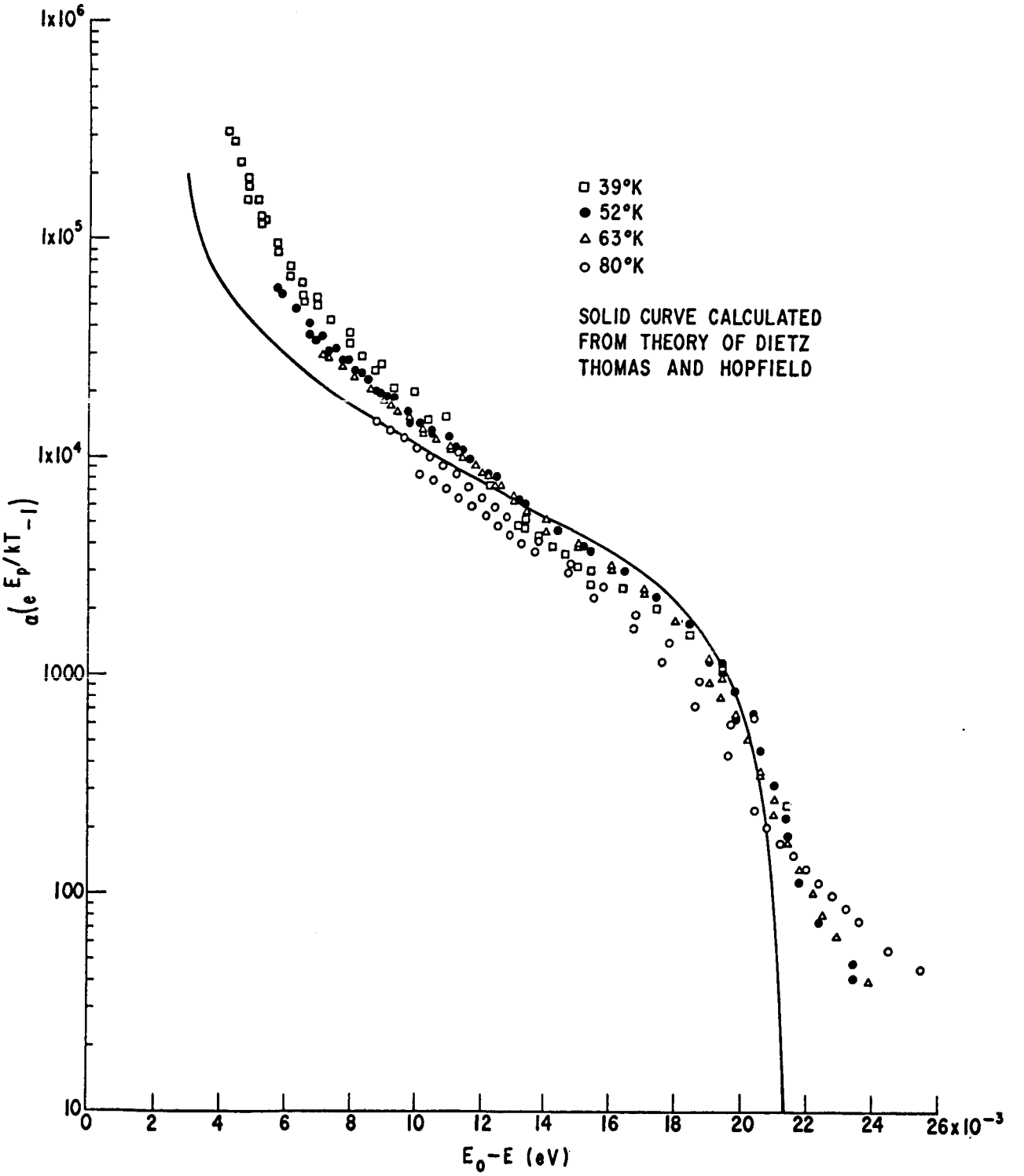

Fig. 4.4 Normalized Absorption Data of Marple[6]

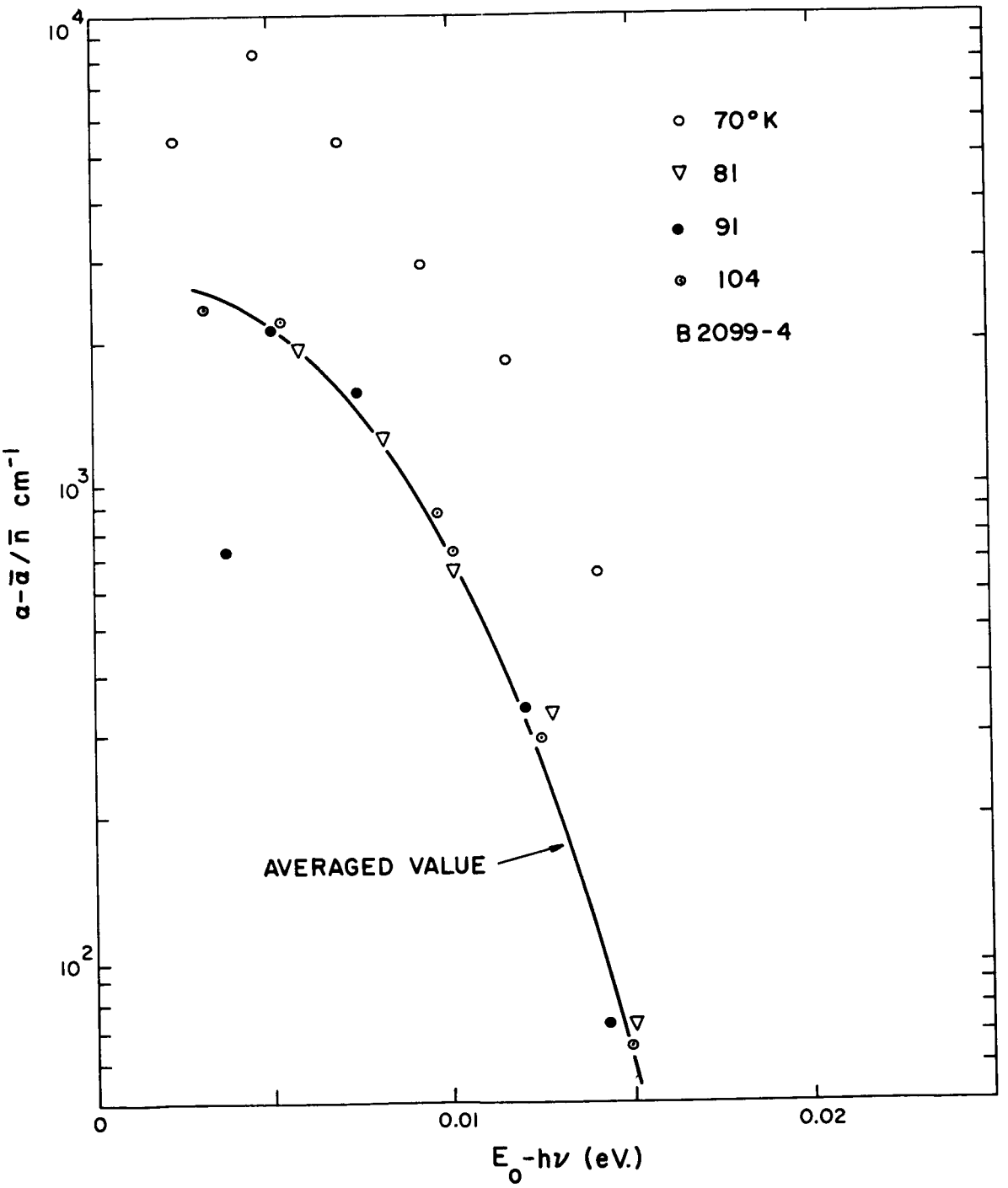

Fig. 4.3 Normalized Absorption at Higher Temperatures

possibility of error in the present study either in spectral calibration or in temperature would seem remote. A mass of data taken over a period of time in which the spectrometer was recalibrated several times, with samples immersed in liquid gases, and for several different samples all are consistent with this observation. This additional data as well as aspects of the measurement and equipment will be reported in detail at the completion of the study.

The significant difference between this and the other investigation appears to be in sample preparation. The data of this study is taken on optically polished samples the other made use of chemically polished surfaces. It would be very surprising if the presumed removal of damage introduced in the polishing process could in fact increase the observed otpical absorption. To resolve this issue, additional experiments are now being instrumented in which polished and chemically prepared samples will be compared.

4.3 Theoretical Aspects of the Absorption Process

A quantitative theory for the absorption by excitons with the assistance of LO phonons has been adapted from the quoted sources.[2,3] However, the derivations are based on a band structure model and contain no adjustable parameter as do the expressions obtained formerly. Further, the interaction of TO phonon modes have been shown to cause a significant contribution to the absorption by excitons at low temperatures. These calculations are lengthy and the expressions are involved, however, the results can be stated quite simply. These, presented the same form as the experimental data of Figure 4.3, are shown in Figures 4.5, 4.6, and 4.7 for three different temperatures.

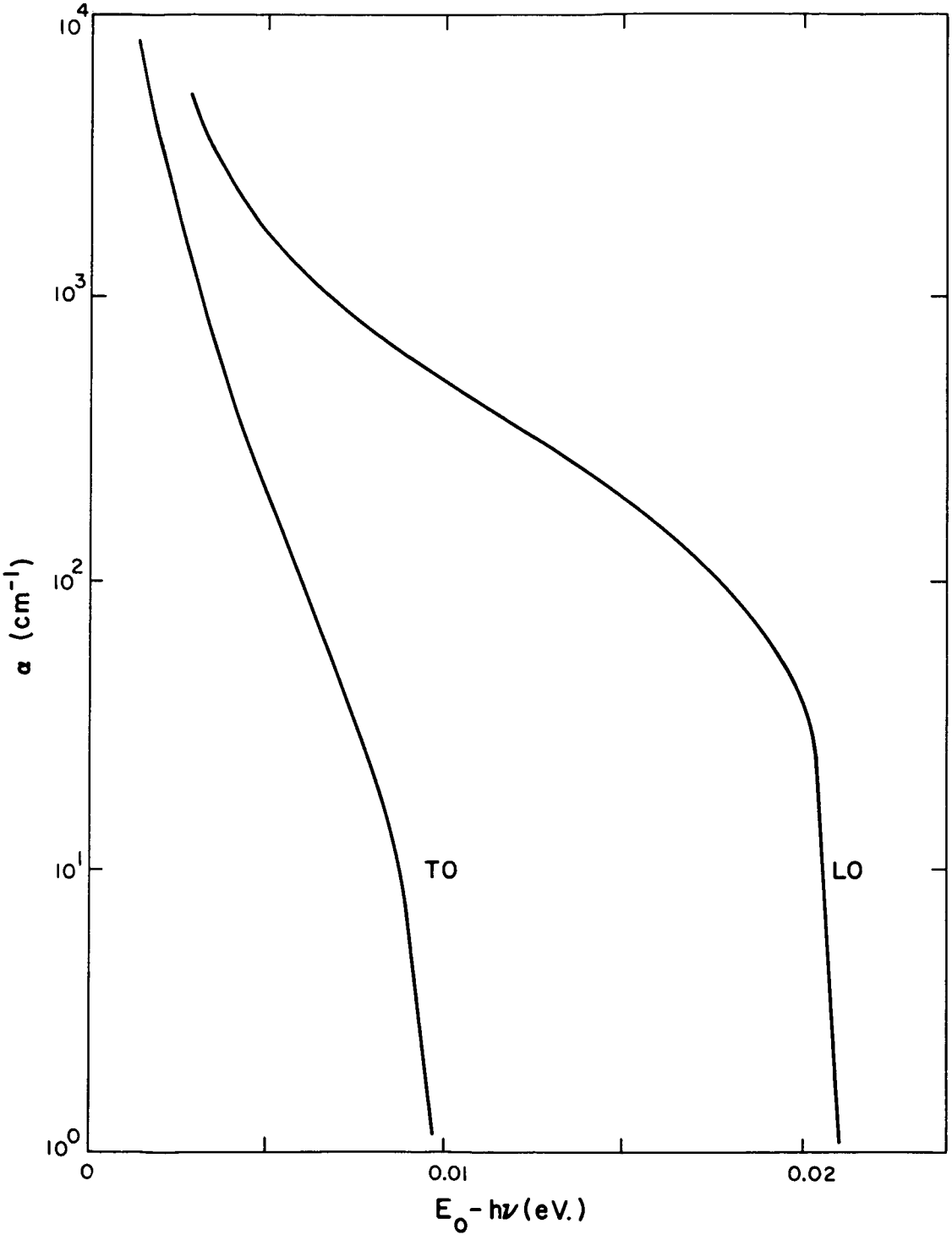

Fig. 4.5 Theoretical Values For $\alpha(E_0 - h\nu)$ For LO and TO Phonon Assisted Absorption by Excitons in CdTe at a Temperature of 70°K

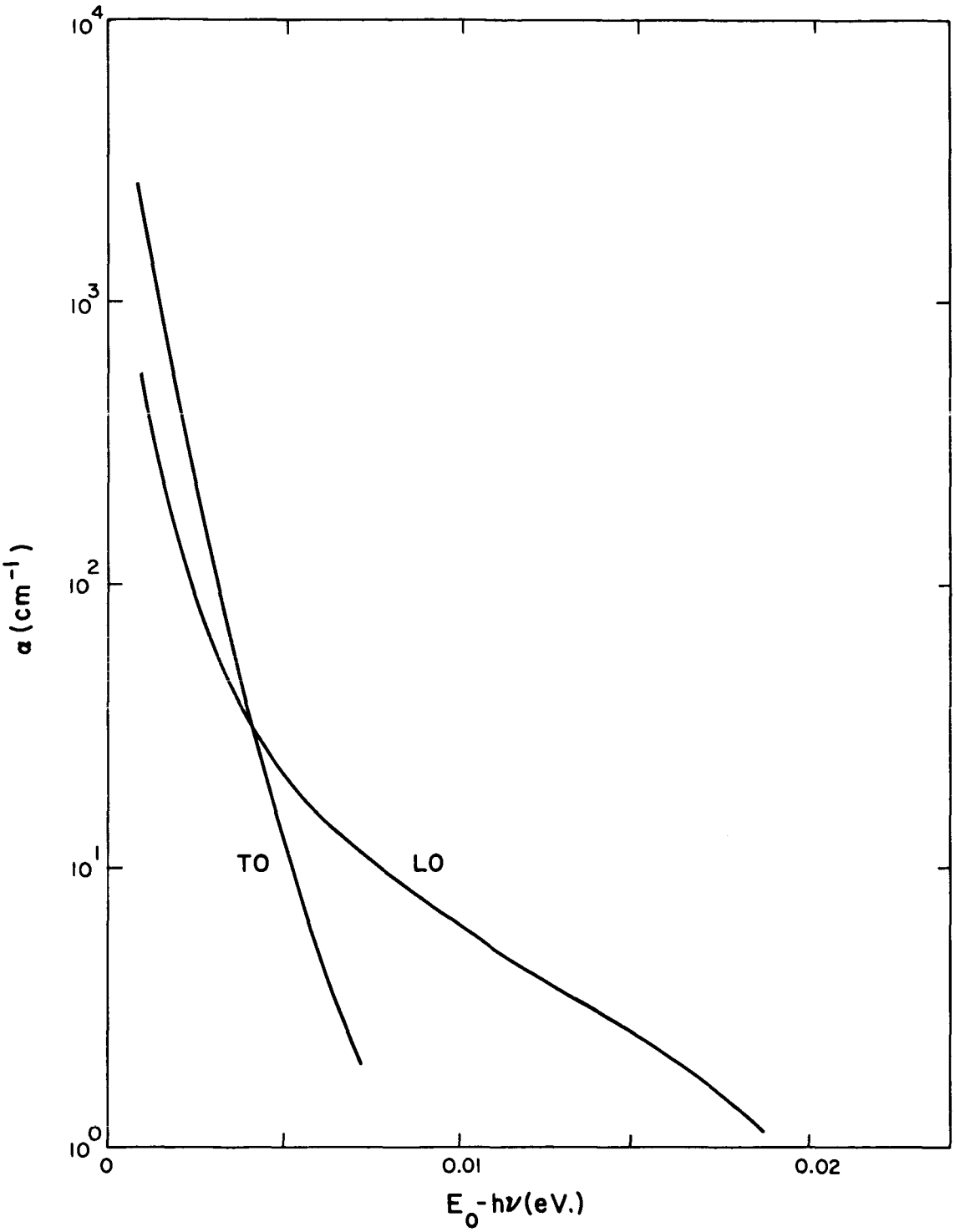

Fig. 4.6 Theoretical Values For $\alpha(E_0 - h\nu)$ For LO and TO Phonon Assisted Absorption by Excitons in CdTe at a Temperature of 31°K

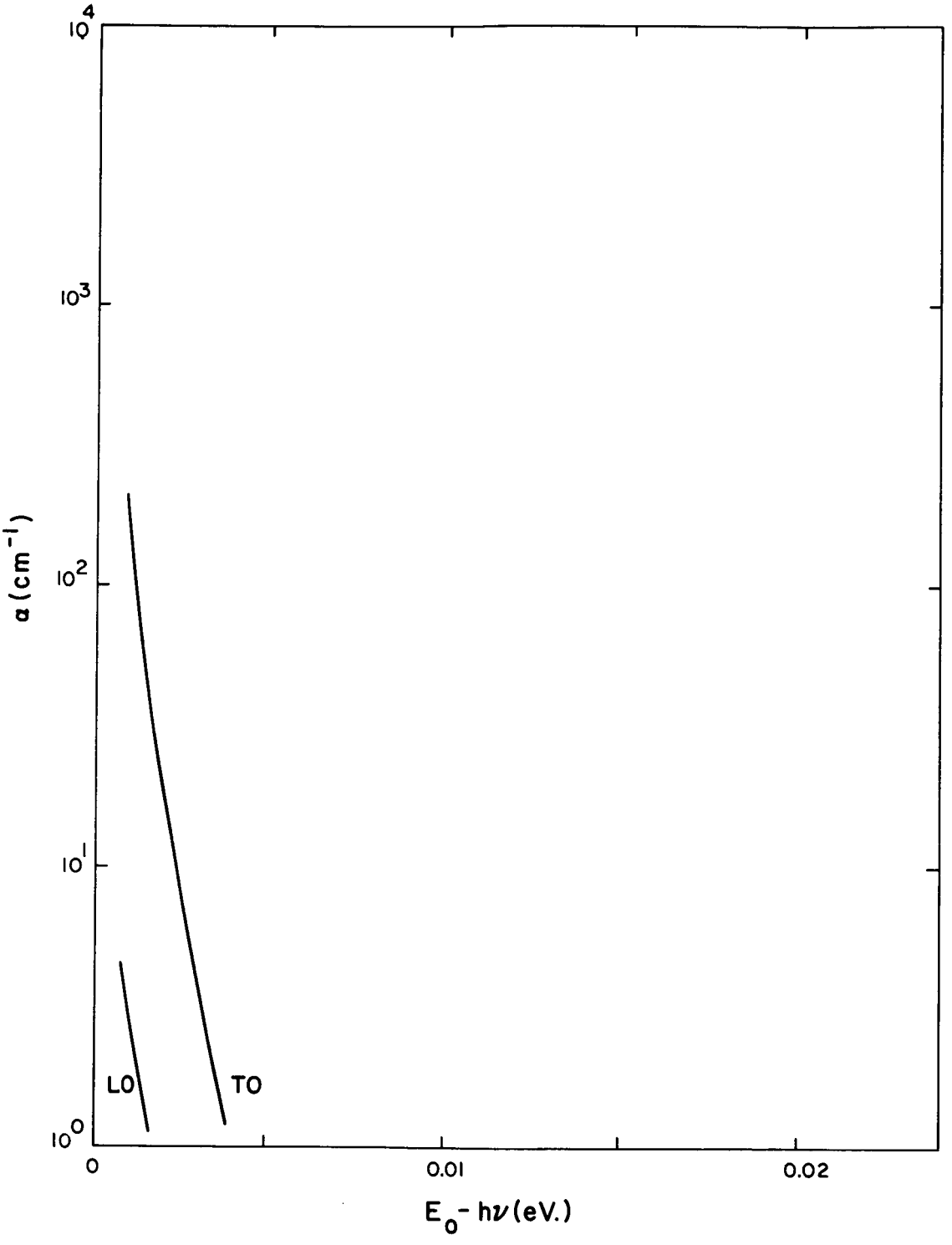

Fig. 4.7 Theoretical Values For $\alpha(E_0 - h\nu)$ For LO and TO Phonon Assisted Absorption by Excitons in CdTe at a Temperature of 17°K

The general method employed to calculate the optical absorption involves a second order time dependent theory. An expression for this as given by Smith[9] is

$$|a_m^{(2)}|^2 = \sum_{n\neq 0} \frac{4|H_{no}|^2|H_{mn}|^2 \sin^2 \frac{1}{2}\omega_{mo}}{\hbar^4 \omega_{no}^2 \omega_{mo}^2}$$

An examination of this theory has shown the correct form to be

$$|a_m^{(2)}|^2 = \frac{1}{\hbar^4}\left| \sum_{n\neq 0} \frac{H_{no} H_{mn}}{\omega_{no}} \right|^2 \frac{\sin^2 \frac{1}{2}\omega_{mot}}{\omega_{mo}^2}$$

The difference is seen to be in the square of the sum rather than in the sum of the squares. This issue arose in the derivation of a TO phonon assisted absorption process where the sum was zero but the sum of the squares was not. The results as based on the former expression were not physically reasonable. This difference has implications on derivation of optical absorption for several different types of processes since intermediate states, written symbolically as n, occur in pairs for a given second order interaction.

4.4 Bibliography

1. "Fundamental Research in Solid State Energy Conversion Processes", Semiannual Technical Summary Report No. 1, November 30, 1963, N.A.S.A. Grant NsG 496 (part), unpublished.

2. Thomas, D.G., J.J. Hopfield, and M. Power, "Excitons and the Absorption Edge of CdS", Phys. Rev. 119, 570 (1960).

3. Dietz, R.E., J.J. Hopfield, and D.G. Thomas, "Excitons and the Absorption Edge of ZnO", J.A.P. 32, 2282 (1961).

4. Marple, D.T.F. and B. Segall, "Optical-Absorption Edge in CdTe: Experimental", Bull. Amer. Phys. Soc. 9, 223 (1964).

5. Segall, B. and D.T.F. Marple, "Optical-Absorption Edge in CdTe: Theoretical", loc, cit.

6. Marple, D.T.F., "Studies of the Optical Absorption Edge in CdTe", unpublished.

7. Davis, P.W. and T.S. Shilliday, "Some Optical Properties of CdTe", Phys. Rev. 118, 1020 (1960).

8. Konak, C. "Some Optical Properties of CdTe", Phys. Status Solidi 3, 1274 (1963).

9. Smith, R.A., "Wave Mechanics of Crystalline Solids", p. 448, Wiley, New York, 1960.

10. Lax, B. and S. Zwerdling, "Magneto-Optical Phenomena in Semiconductors", Progress in Semiconductors, p. 221 Vol. V, Wiley, New York, 1960.

11. Halsted, R.E. unpublished data.

P.J. Shaver, R.Z. Bachrach

5.0 THERMAL AND ELECTRONIC TRANSPORT PROPERTIES OF ZINC ANTIMONIDE

5.1 Introduction

Zinc antimonide is a semiconducting compound that is a useful component of thermoelectric power generating systems that operate at moderate temperatures. Previous thermoelectric optimizations of zinc antimonide have been largely empirical due to difficulties encountered in growing single crystals of this material. The basic transport properties of zinc antimonide are under study experimentally and fitted to a theoretical model. Work has progressed during the last reporting period in the areas of crystal growth, sample preparation, and equipment development for thermal and electronic properties evaluation. Data on the anisotropic coefficients of thermal expansion and preliminary galvanomagnetic data are now available.

5.2 Crystal Growth

The horizontal zone recrystallization technique is still being used to produce ZnSb. Early crystals were grown in evacuated quartz ampoules, following the technique of other workers.[1] However, as the material handling procedures were improved so that the surfaces of the ingots were much cleaner during crystal growth, a persistent and serious decomposition of the ingots set in.

This decomposition was evidenced by the condensing of considerable quantities of material on the cooler walls of the containing ampoule and by the mechanical warping of the zone recrystallized portion of the ingot. A quantitative chemical anlaysis of samples of distillate taken from the walls

---

1. Eisner, Mazelsky and Tiller, J. Appl. Phys., 31, 1832, (1961).

of four different ampoules indicated the presence of both antimony and zinc with a zinc content of between 51 to 55 At % (± 1%).

It was found that this decomposition could be suppressed by replacing the 5 x 10^{-6} Torr. room temperature vacuum in the growth ampoules by a room temperature pressure of one atmosphere of either nitrogen or argon. Argon is currently being used.

The currently produced ingots often contain a number of low angle grain boundaries (on the order of six to ten per ingot). These boundaries generally extend the length of the ingot (8 to 15 cm), often have a common axis which coincide with the growth direction, and have a relative mis-orientation of one to two degrees. Efforts are being made to reduce low angle boundary formation by carbonizing the walls of the containment ampoule, adjusting the geometry of the freezing interface, and by changing the crystallographic growth direction to other principal axes. The current growth axis approximately coincides with the <001> direction.

Currently produced undoped crystals are p-type with carrier concentrations on the order of 1 x 10^{-16} cm^{-3}. It has been found possible to control the hole concentration by using a single zone pass (the growth pass) of a copper doped molten zone. All of the crystals grown thus far show a ± 3 percent variation of thermoelectric power along an 8 to 15 cm. length. The thermo-electric power is measured at room temperature on an approximate (100) face.

Aluminum, selenium, and indium doped ingots are being produced in an effort to grow n-type crystals. Several aluminum and selenium doped samples have been produced, but were all p-type.

5.3 Sample Preparation

ZnSb monocrystals have been found to be too brittle to be reliably cut

by conventional diamond saws without considerable risk of fracture. Thus, the spark erosion cutting technique has been used to section ZnSb monocrystals. ZnSb is readily cut by this method.

It has been found that ordinary 60-40 lead-tin solder makes ohmic electrical contacts to ZnSb when applied with a rosin flux. Pure lead has also been used with rosin flux to produce ohmic contacts to ZnSb.

5.4 Electrical and Thermal Measurements

A number of initial galvanomagnetic measurements have been made. The results of magnetoresistance measurements as yet are not conclusive enough to report in detail. However, initial measurements have indicated that the longitudinal magnetoresistance vanishes along the b and c directions. Longitudinal magnetoresistance experiments in the a direction have not been attempted as yet. These preliminary magnetoresistance results indicate that the constant energy surfaces of the ZnSb valence band might be theoretically characterized as one, or more, general ellipsoids aligned with principal axes coincident with the principal axes of the crystal. Figure 5.1 shows a typical result for the temperature variation of the Hall coefficient and electrical resistivity for one crystal orientation.

Apparatus is being readied for thermal conductivity measurements.

Work to develop an rf dilatometer has progressed successfully. The r-f dilatometer has a short-term resolution of 600 Å and a long term resolution of 1100 Å. A temperature range from -195 to 1000 °C can be obtained.

Thermal expansion in one single crystal of ZnSb was found to be quite anisotropic. The principal thermal expansion coefficients of one ZnSb crystal are presented in Table 5.1 along with measurement results for aluminum

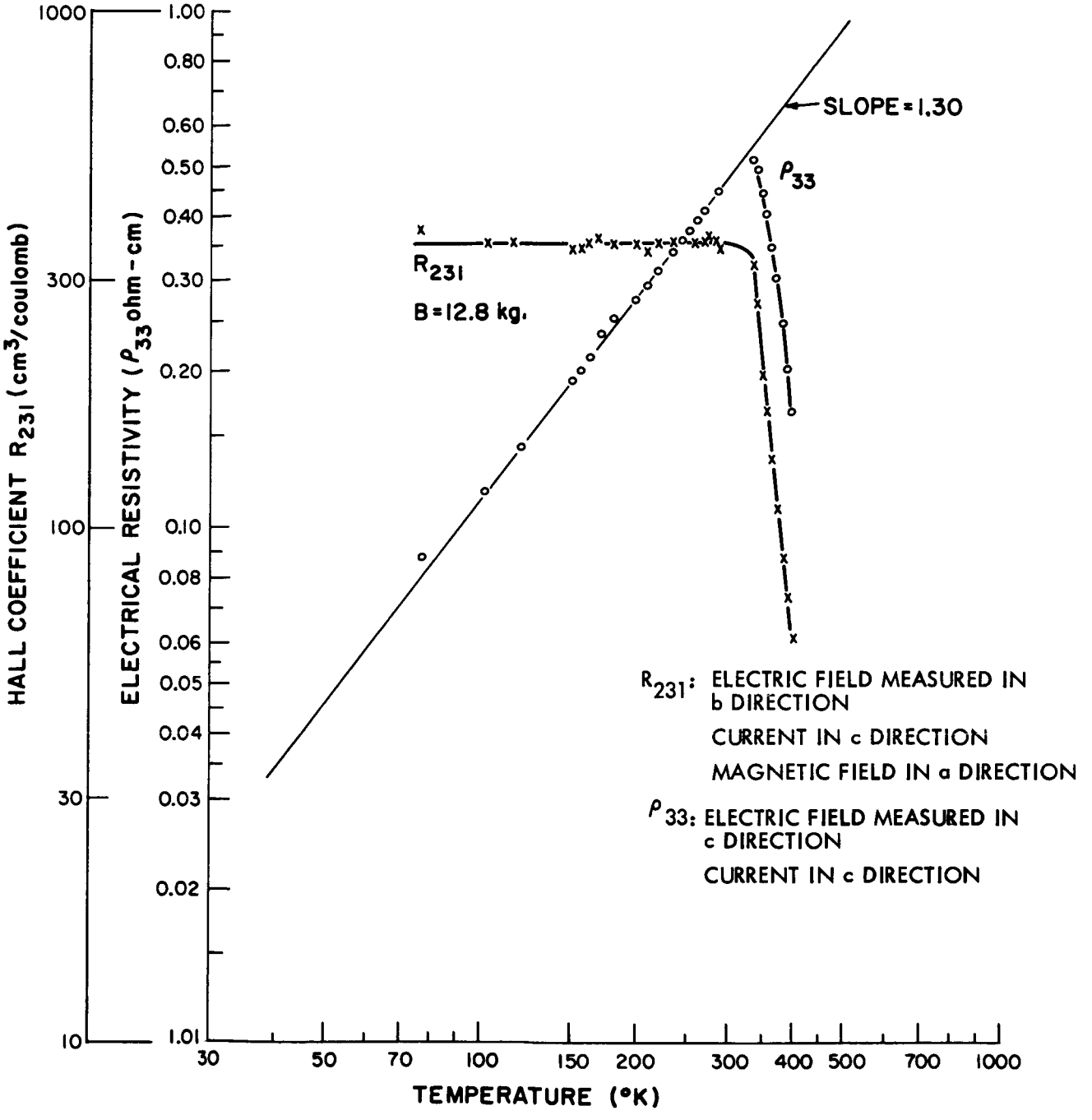

Fig. 5.1 Representative Temperature Dependences of Electrical Resistivity and Hall Coefficient

Material		100°C	200°C	300°C	Sample Length
ZnSb	<100>	$15.6 \times 10^{-6} (°K)^{-1}$	$18.5 \times 10^{-6} (°K)^{-1}$	$17.2 \times 10^{-6} (°K)^{-1}$	.157"
	<010>	6.7	6.7	6.7	.403
	<001>	1.5	1.4	1.7	.399"
	a_v	23.8	26.6	27.6	
Al		23.2	23.2	300° 14.5 400° 22.4	.782"
Ge		7.6	5.3	6.9	.364"

Table 5.1 Measured Linear Thermal Expansion Coefficients at Several Temperatures.

and germanium. These results are believed to have an accuracy of $\pm$ 10%. The results for germanium and aluminum agree with published values. Figure 5.2 presents the thermal expansivity of these samples versus temperature. The linear thermal expansion coefficients are the slopes of these curves.

The following identification of the crystallographic axes is made in this work:

$$\langle 100 \rangle = a_o = \text{"1"} = 6.20\ \text{Å}$$

$$\langle 010 \rangle = b_o = \text{"2"} = 7.74\ \text{Å}$$

$$\langle 001 \rangle = c_o = \text{"3"} = 8.10\ \text{Å}$$

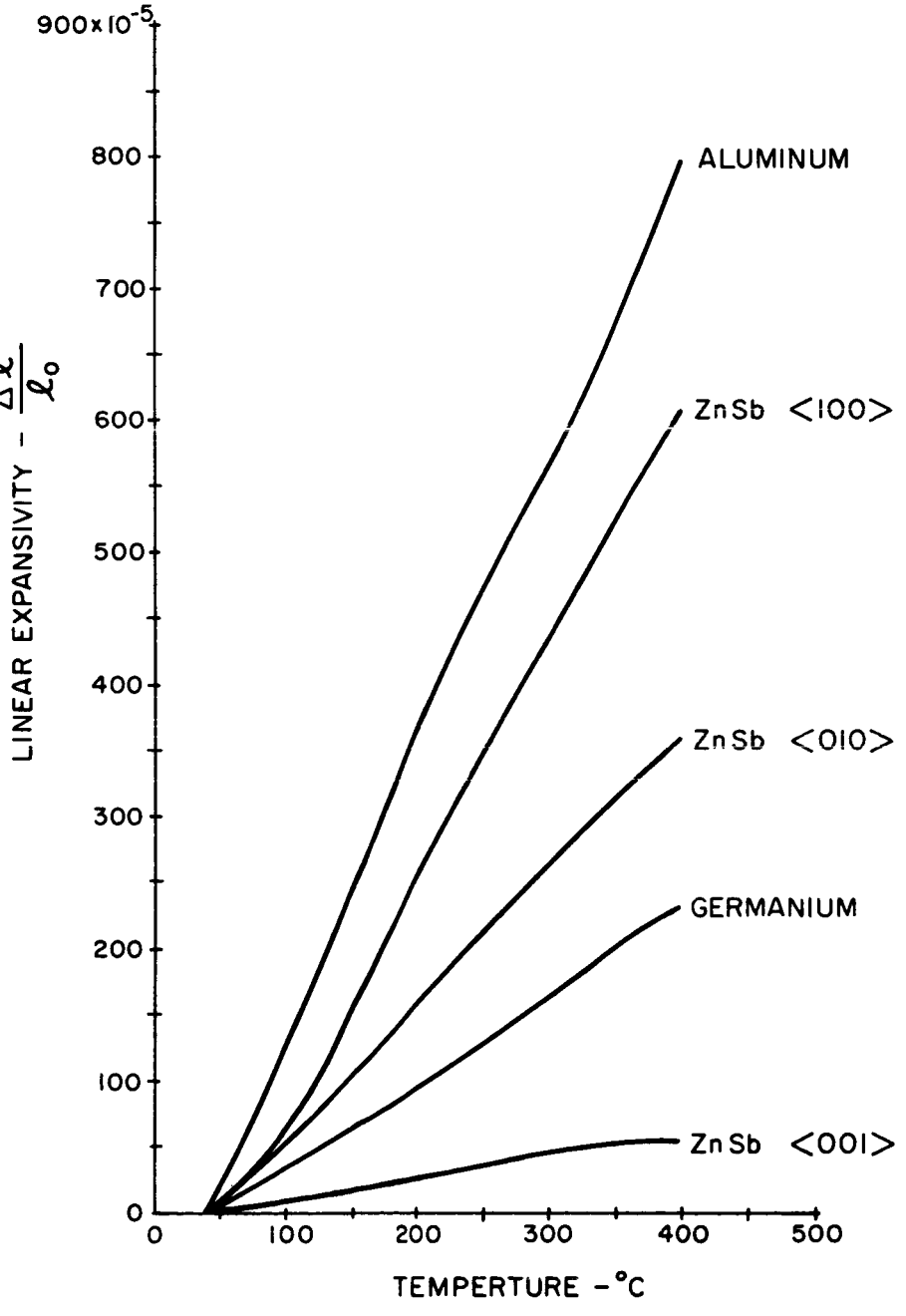

Fig. 5.2 Measured Linear Expansivity vs. Temperature

6.0 THE INFINITE-STAGE ETTINGSHAUSEN COOLER

This study is concerned with the performance of a bismuth infinite-stage Ettingshausen cooler at liquid nitrogen temperature. The experimental work involved the growth of single crystal bismuth by a rapid freeze method, the shaping of single crystal bismuth by a spark erosion cutting process, the design and implementation of a sample-holder, the implementation of a current supply for the cooler and measuring apparatus for the test work, and the actual testing of the device.

High purity, unstrained, striation free, single crystal bismuth was needed for the cooler; and, at the beginning of this work, the only method of obtaining this high quality material was to grow it from zone-refined bismuth, using a quick freeze technique developed by Sidney Fischler at M.I.T. Lincoln Laboratory. 1/8 inch slabs of bismuth were successfully grown by this technique; however, attempts of increasing the thickness of these slabs were unsuccessful. Since bismuth of a larger thickness could not be grown, single crystal bismuth donated by Mr. Fischler was used for the remaining portion of this work.

The exponential shaping of the cooler was achieved by a spark erosion cutting technique at Lincoln Laboratory. A tungsten wire (20 gauge) template was used to make an exponential cooler with a shaping ratio of 100:1. Due to difficulty in cutting out the narrow portion of the contour, this portion came out jagged, with a resulting effective shaping ratio of 50:1.

A quartz box, attached to the end of quartz tubing, was to be used as the sample-holder. The box, with a rectangular opening for the sample was to be evacuated, with the sample making a pressure fitting. The system was then to be lowered into a liquid-nitrogen filled dewar, located between the pole pieces of an electromagnet. Many problems existed with this

holder in making a good pressure fitting with the sample, and ultimately, a plexiglass sample-holder, similar in design, was used.

A current supply, constructed of automobile batteries in series with a variable carbon resistor, was used to provide a 0-25 ampere current for a duration of 5 seconds. A silicon controlled rectifier was used to trigger the current on, and a relay, triggered by a 5-second servo timer, turned the current off.

A ΔT of 2 1/2° was obtained from an exponentially shaped cooler with a shaping ratio of 50:1, using an input current of 25 amperes and a 10.7 kilogauss magnetic field. The sample had been fractured before testing, and, since strains in bismuth usually reduce the performance drastically, it was not surprising that this cooler did not achieve the theoretical ΔT of 15°. It is expected that a cooler of unstrained bismuth would have a much better performance at liquid nitrogen temperature.

This work was carried out under the support of the Hughes Aircraft Company, Aerospace Group under the auspices of the Hughes Masters Fellowship Program. Thanks are due to the staff of Lincoln Laboratory for their help, in particular to T.C. Harman and S. Fischler.